iScience

CellPress
OPEN ACCESS

Article

Host-microbiome interactions in distinct subsets of preterm labor and birth

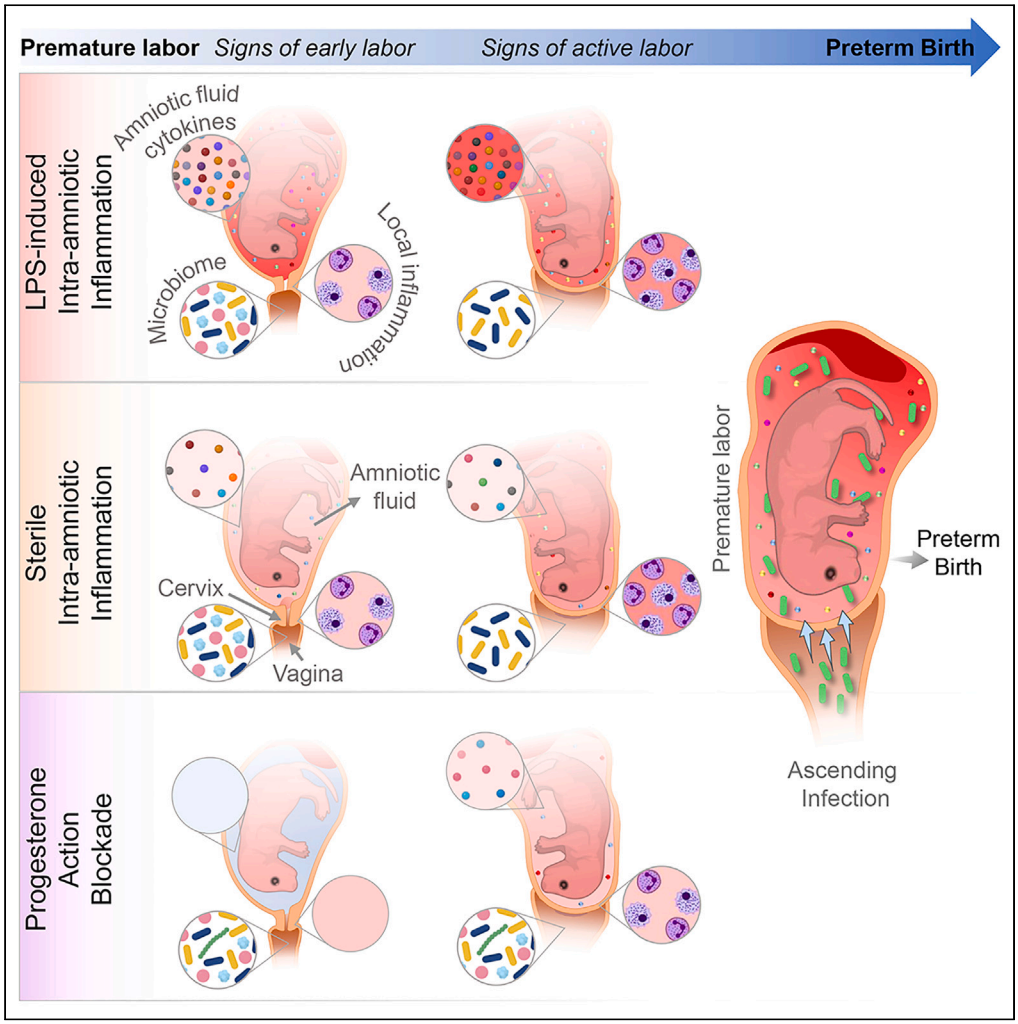

Jose Galaz, Roberto Romero, Jonathan M. Greenberg, ..., Tomi Kanninen, Valeria Garcia-Flores, Nardhy Gomez-Lopez

romeror@mail.nih.gov (R.R.)
nardhy@wustl.edu (N.G.-L.)

Highlights

Different preterm birth subsets display distinct host-microbiome profiles

Intra-amniotic IL-1α and LPS induce inflammation and disrupt the vaginal microbiome

RU-486 triggers local immune responses without altering the vaginal microbiome

Preterm labor permits bacterial ascension from the vagina into the amniotic cavity

Galaz et al., iScience 26, 108341
December 15, 2023 © 2023
https://doi.org/10.1016/j.isci.2023.108341

iScience

CellPress
OPEN ACCESS

Article

Host-microbiome interactions in distinct subsets of preterm labor and birth

Jose Galaz,[1,2,3] Roberto Romero,[1,4,5,*] Jonathan M. Greenberg,[1,2] Kevin R. Theis,[1,2,6] Marcia Arenas-Hernandez,[1,2] Yi Xu,[1,2] Marcelo Farias-Jofre,[1,2,3] Derek Miller,[1,2,7] Tomi Kanninen,[1,2] Valeria Garcia-Flores,[1,2,7] and Nardhy Gomez-Lopez[1,2,6,7,8,9,10,*]

SUMMARY

Preterm birth, the leading cause of perinatal morbidity, often follows premature labor, a syndrome whose prevention remains a challenge. To better understand the relationship between premature labor and host-microbiome interactions, we conducted a mechanistic investigation using three preterm birth models. We report that intra-amniotic delivery of LPS triggers inflammatory responses in the amniotic cavity and cervico-vaginal microenvironment, causing vaginal microbiome changes and signs of active labor. Intra-amniotic IL-1α delivery causes a moderate inflammatory response in the amniotic cavity but increasing inflammation in the cervico-vaginal space, leading to vaginal microbiome disruption and signs of active labor. Conversely, progesterone action blockade by RU-486 triggers local immune responses accompanying signs of active labor without altering the vaginal microbiome. Preterm labor facilitates ascension of cervico-vaginal bacteria into the amniotic cavity, regardless of stimulus. This study provides compelling mechanistic insights into the dynamic host-microbiome interactions within the cervico-vaginal microenvironment that accompany premature labor and birth.

INTRODUCTION

Preterm birth, the leading cause of morbidity and mortality under five years of age,[1,2] is defined as birth occurring before 37 weeks of gestation.[2,3] The rate of preterm birth in the United States has increased over the last decade,[4] resulting in a high societal burden.[5–7] Such a sustained increase may be partially due to the continued lack of understanding of the complex mechanisms leading to preterm birth. Two-thirds of preterm births are preceded by premature labor,[8] a syndrome of multiple etiologies that includes intra-amniotic infection and intra-amniotic inflammation, decline in progesterone action, cervical disease, and stress, among others.[9] Among the known and proposed etiologies, intra-amniotic inflammation and a blockade of progesterone action have been causally linked to premature labor and subsequent preterm birth.[10–26] Intra-amniotic inflammation can be induced by microbes ascending from the lower genital tract into the amniotic cavity (i.e., microbial intra-amniotic inflammation or intra-amniotic infection)[27–31] or by alarmins (i.e., endogenous danger signals).[32,33] The latter is a recently discovered pathology termed sterile intra-amniotic inflammation.[34–39] Importantly, sterile intra-amniotic inflammation is more frequent than microbial intra-amniotic inflammation in women with premature labor and intact membranes[36] as well as in women with a mid-trimester sonographic short cervix.[37] Notably, the blockade of progesterone action using the progesterone receptor antagonist RU-486 induces preterm birth in mice in the absence of a massive inflammatory response in the amniotic cavity.[40] These findings suggest that the mechanisms of disease underlying intra-amniotic inflammation (either microbial or sterile) differ in nature from those involving the blockade of progesterone action; however, no direct comparison among these three different models of premature labor has been undertaken.

The cervico-vaginal microenvironment has been an area of focus for investigations aimed at identifying biomarkers to predict preterm birth.[41–46] Yet, the performance of predictive models using the cervico-vaginal microbiome and/or immune response has been modest[47] and only allows for the prediction of a subset of preterm birth cases.[48,49] One potential explanation for this conundrum is the unknown causal

[1]Pregnancy Research Branch, Division of Obstetrics and Maternal-Fetal Medicine, Division of Intramural Research, *Eunice Kennedy Shriver* National Institute of Child Health and Human Development, National Institutes of Health, U.S. Department of Health and Human Services (NICHD/NIH/DHHS), Bethesda, MD 20892, USA
[2]Department of Obstetrics and Gynecology, Wayne State University School of Medicine, Detroit, MI 48201, USA
[3]Division of Obstetrics and Gynecology, School of Medicine, Faculty of Medicine, Pontificia Universidad Catolica de Chile, Santiago 8330024, Chile
[4]Department of Obstetrics and Gynecology, University of Michigan, Ann Arbor, MI 48109, USA
[5]Department of Epidemiology and Biostatistics, Michigan State University, East Lansing, MI 48824, USA
[6]Department of Biochemistry, Microbiology, and Immunology, Wayne State University School of Medicine, Detroit, MI 48201, USA
[7]Department of Obstetrics and Gynecology, Washington University School of Medicine, St. Louis, MO 63110, USA
[8]Center for Molecular Medicine and Genetics, Wayne State University, Detroit, MI 48201, USA
[9]Department of Pathology and Immunology, Washington University School of Medicine, St. Louis, MO 63110, USA
[10]Lead contact
*Correspondence: romeror@mail.nih.gov (R.R.), nardhy@wustl.edu (N.G.-L.)
https://doi.org/10.1016/j.isci.2023.108341

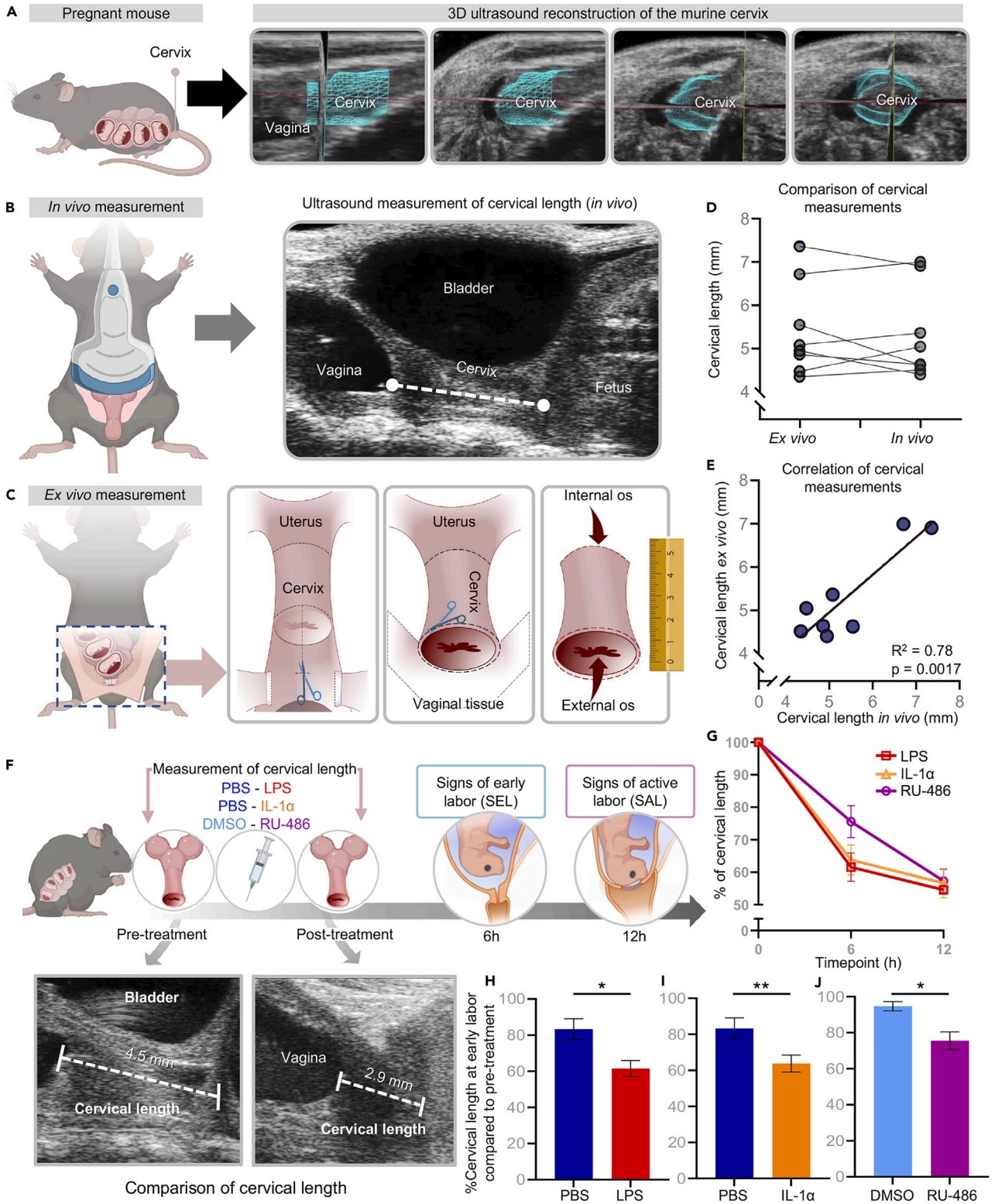

Figure 1. A non-invasive approach to detect signs of early premature labor and active premature labor

(A) Representative high-resolution ultrasound images showing multiple views from a 3D reconstruction of the murine cervix (turquoise).

(B) Experimental design showing the measurement of cervical length *in vivo* using high-resolution ultrasound (n = 8 dams) and (C) the collection of the cervix after the ultrasound scan to measure cervical length *ex vivo*.

Figure 1. *Continued*

(D) Paired dot plot comparing cervical length as measured *in vivo* and *ex vivo*.

(E) Correlation of *in vivo* and *ex vivo* cervical length measurements.

(F) Initial cervical length was measured by using high-resolution ultrasound followed by the intra-amniotic injection of PBS, LPS, or IL-1α, or the subcutaneous injection of DMSO or RU-486 (n = 6–9 dams per group). Cervical length was measured again with signs of early premature labor (SEL; 6 h) or signs of active premature labor (SAL; 12 h).

(G) Plot showing the trend of cervical shortening from the initial measurement (no labor) to signs of early (6 h) and active (12 h) premature labor. Symbols represent the mean and whiskers represent the SEM. Bar plots showing cervical shortening represented as a percentage of the initial measurement in (H) LPS-induced intra-amniotic inflammation, (I) sterile intra-amniotic inflammation (IL-1α), and (J) progesterone action blockade (RU-486). Bars represent means, and whiskers represent standard deviation. p values were determined by Mann-Whitney U tests. *p < 0.05; **p < 0.01. See also Figure S1 and Video S1.

relationship between different subsets of premature birth and changes in the cervico-vaginal microbiome as well as the accompanying inflammatory response.

In the current study, we used established models of preterm birth, namely, LPS-induced intra-amniotic inflammation, sterile intra-amniotic inflammation, and progesterone action blockade, to develop and validate an ultrasound-based non-invasive approach to detect signs of early and active premature labor. Next, we investigated the nature and temporal dynamics of the intra-amniotic inflammatory response during each type of premature labor. We also evaluated whether each type of premature labor induces changes in the vaginal microbiome that accompany signs of early and active premature labor and whether such changes are accompanied by leukocyte infiltration and structural or inflammatory responses in the cervix. Last, we evaluated whether premature labor can facilitate the ascension of bacteria from the vagina into the amniotic cavity. This study provides mechanistic evidence of the dynamic cervico-vaginal host-microbiome interactions during different pathological processes leading to premature labor, knowledge that might be utilized to improve the investigation of non-invasive biomarkers for preterm birth.

RESULTS

A non-invasive approach to detect signs of early and active premature labor

The common pathway of labor includes the processes of myometrial contraction, cervical remodeling, and membrane/decidual activation, whose orchestrated initiation culminates in the delivery of a preterm or a term neonate.[9,50–53] The diagnosis of labor relies on the clinical manifestation of uterine contractions and cervical dilatation in humans[54]; however, the identification of such processes in mice requires excision of the cervico-uterine tissues for *ex vivo* experimentation or the use of invasive methods.[55–57] Therefore, we first established a non-invasive approach to determine cervical shortening as a readout of premature labor in mice. Pregnant mice underwent a *trans*-abdominal ultrasound to monitor cervical changes as evidenced in the representative images taken from a 3D reconstruction video (Figure 1A, Video S1, and STAR Methods). High-resolution ultrasound was utilized to measure cervical length *in vivo* (Figure 1B). Immediately following ultrasound evaluation, the cervix was carefully collected to repeat this measurement *ex vivo* (Figure 1C). No differences were found between the cervical length measured by ultrasound *in vivo* and the *ex vivo* determination (Figure 1D), which was reflected by a strong positive correlation between the measurements obtained using these methods (Figure 1E). The first stage of the physiologic labor process involves an early or latent phase followed by an active phase, leading to the second stage of labor that results in delivery of the fetus.[58,59] Therefore, having established an accurate *in vivo* approach to evaluate cervical length in mice, we next identified signs of early premature labor (SEL) and signs of active premature labor (SAL) in a reliable model of intra-amniotic inflammation-induced preterm birth, in which premature parturition is induced by the ultrasound-guided intra-amniotic injection of the microbial product LPS.[16,17,24] Given that the interval between injection to delivery was similar between the LPS model and the other two models of preterm birth (intra-amniotic injection of the alarmin IL-1α represents a model of preterm birth induced by sterile intra-amniotic inflammation,[20] and subcutaneous administration of RU-486 represents a model of preterm birth caused by the blockade of progesterone action[40]; Table S1), we reasoned that the cervical length determinations would be applicable among models. The SEL corresponded to the earliest time point when cervical shortening could be accurately determined using the ultrasound method (6 h post-injection), whereas SAL corresponded to the time point close to the earliest observed preterm delivery (12 h post-injection) (Figure 1F). Using these parameters, we identified SEL and SAL in all three models: LPS-induced intra-amniotic inflammation (Figures 1G, 1H, and S1A), sterile intra-amniotic inflammation (Figures 1G, 1I, and S1B), and progesterone action blockade (Figures 1G, 1J and S1C). As expected, the cervix was shorter in active than in early premature labor across all three models (Figure 1G). It is worth noting that uterine contraction-like movements were detected accompanying SAL (Video S2), supporting the diagnosis of labor. Taken together, these results show that the non-invasive determination of cervical shortening is attainable in mice and that this approach allows for identifying signs of early and active premature labor preceding preterm birth.

LPS, IL-1α, and RU-486 trigger distinct intra-amniotic inflammatory responses accompanying signs of early premature labor and active premature labor

Having established signs of early and active premature labor in the three different models of preterm birth, we next explored the nature of the inflammatory response in the amniotic cavity during these two time points of parturition. Samples of amniotic fluid were collected with SEL or SAL to evaluate the concentrations of 36 immune mediators (Figure 2A, STAR Methods). The intra-amniotic injection of LPS induced a massive inflammatory response in the amniotic cavity with both SEL and SAL; however, such responses were distinct (Figures 2B, 2C, S2, S3A, and S3B). With SEL, the amniotic fluid concentrations of M-CSF, GM-CSF, CCL7, and CCL11 were greater upon LPS administration compared to

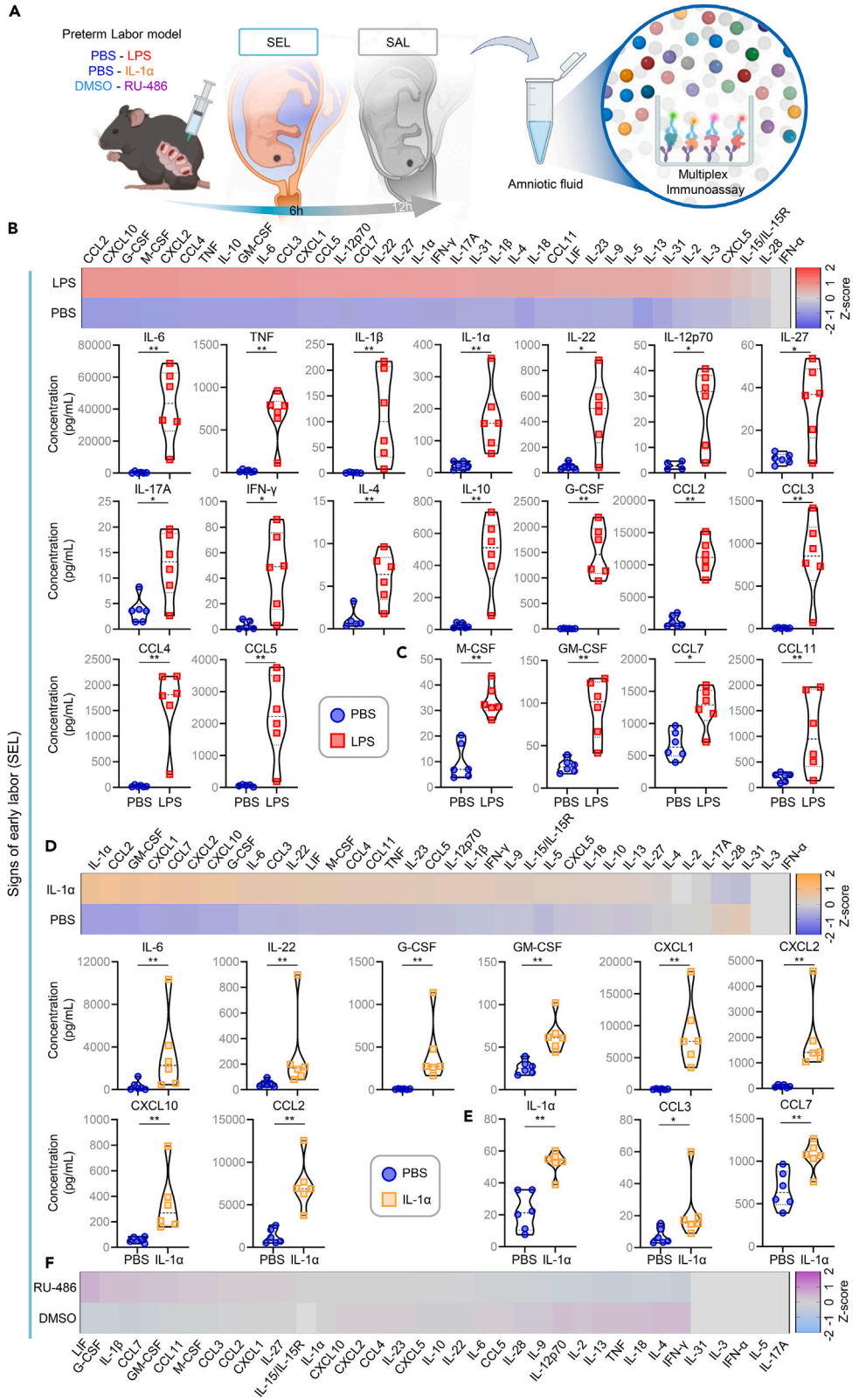
A
Preterm Labor model
PBS - LPS
PBS - IL-1α
DMSO - RU-486
SEL
SAL
6h
12h
Amniotic fluid
Multiplex Immunoassay
B
LPS
PBS
Z-score
Concentration (pg/mL)
PBS
LPS
C
D
IL-1α
PBS
E
F
RU-486
DMSO
Signs of early labor (SEL)

Figure 2. LPS, IL-1α, and RU-486 trigger distinct intra-amniotic inflammatory responses with signs of early premature labor or active premature labor

(A) Dams were intra-amniotically injected under ultrasound guidance with PBS, LPS, or IL-1α, or subcutaneously with DMSO or RU-486. Amniotic fluid was collected with signs of early premature labor (SEL; 6 h; n = 6 dams per group) or signs of active premature labor (SAL; 12 h; n = 9–10 dams per group), and multiple cytokines/chemokines were measured using a multiplex immunoassay.

(B) Heatmap representation and individual plots showing the amniotic fluid concentrations of cytokines/chemokines with SEL in dams injected with PBS or LPS.

(C) Individual plots of immune mediators that were exclusively increased with SEL induced by LPS.

(D) Heatmap representation and individual plots showing the amniotic fluid concentrations of cytokines/chemokines with SEL in dams injected with PBS or IL-1α.

(E) Individual plots of immune mediators that were exclusively increased with SEL induced by IL-1α.

(F) Heatmap representation showing the amniotic fluid concentrations of cytokines/chemokines with SEL in dams injected with DMSO or RU-486.

Data are shown as heatmaps representing the mean of the *Z*-score of each cytokine/chemokine and violin plots where dashed midlines indicate medians and dotted lines indicate interquartile ranges. p values were determined by Mann-Whitney U tests. *p < 0.05; **p < 0.01. See also Figures S2 and S3.

PBS-injected controls (Figure 2C); yet, such immune mediators were not increased with SAL (Figure S3A). On the other hand, the amniotic fluid concentrations of IL-2, IL-13, IL-28, and CXCL5 were increased with SAL induced by LPS (Figure S3B) but not with SEL (Figure 2B). Furthermore, the LPS-induced increase in the concentrations of several cytokines (e.g., TNF, IL-1β, IL-27, IL-4, IL-5, IL-10, and IL-31) was greater with SAL than with SEL (Figures 2B, S2, and S3A). The intra-amniotic inflammatory response induced by IL-1α was milder than that induced by LPS (Figures 2B, 2C, S2, S3A, and S3B vs. Figures 2D, 2E, S3C, and S3D), consistent with amniotic fluid cytokine determinations in pregnant women with either sterile or microbial intra-amniotic inflammation.[60,61] Moreover, SEL and SAL triggered by IL-1α were characterized by increased amniotic fluid concentrations of specific cytokines (Figures 2D and 2E vs. Figures S3C and S3D). For example, the intra-amniotic injection of IL-1α induced an increase in the amniotic fluid concentrations of IL-1α, CCL3, and CCL7 with SEL (Figure 2E), but this was not observed with SAL (Figure S3C). IL-1α also induced a rise in the amniotic fluid concentrations of CXCL5 and M-CSF solely with SAL (Figure S3D). Notably, RU-486 injection did not trigger an intra-amniotic inflammatory response with SEL and only induced an increase in two inflammatory mediators, IL-6 and CCL2, with SAL (Figures 2F and S3E), suggesting that such a mild intra-amniotic inflammatory response could be a consequence of the process of parturition. Together, these data show that microbial products, alarmins, and progesterone action blockade each trigger inflammatory responses in the amniotic cavity that differ in both intensity and nature and that intra-amniotic inflammation can be both a cause and a consequence of the onset of premature labor.

The vaginal microbiome changes with signs of active premature labor solely in the presence of intra-amniotic inflammation

The traditional view is that changes in the vaginal microenvironment precede the onset of premature labor; therefore, the assessment of the local microbiome or immune response will serve to generate biomarkers to identify women who ultimately delivered a preterm neonate.[47] Recently, we generated evidence showing that such an approach serves only to identify a subset of women who will experience spontaneous preterm birth, namely, those with preterm prelabor rupture of membranes (PPROM).[48,49] Interestingly, the intra-amniotic inflammatory response of women with PPROM is strong,[62–64] and this subset of patients is more likely to experience infection of the amniotic cavity caused by ascension of vaginal bacteria.[38,65,66] However, it is unknown whether said alterations in the vaginal microbiome are a cause or a consequence of the intra-amniotic inflammatory response. Therefore, we investigated whether changes in the vaginal microbiome occur before or together with SAL, where the intra-amniotic inflammatory response is more accentuated in the LPS-induced intra-amniotic inflammation model of preterm birth (Figure S3A). We also explored the relationship between the vaginal microbiome and intra-amniotic inflammation in the sterile intra-amniotic inflammation and progesterone action blockade models of preterm birth. To address these research questions, a vaginal swab was taken from dams without labor prior to administration of the stimulus to induce preterm birth, and a second vaginal swab was taken with SEL (Figure 3A, STAR Methods) or SAL (Figure 4A, STAR Methods) to study the vaginal microbiome, using 16S rRNA gene sequencing.

With SEL, neither intra-amniotic LPS nor intra-amniotic IL-1α altered bacterial diversity in the vagina as measured by richness (Figures 3B and 3E) or by bacterial composition and structure (Figures 3C and 3F; Table S2). The taxonomic identities of the two most prominent (≥2% average relative abundance) amplicon sequence variants (ASVs) for both the LPS and IL-1α groups were *Rodentibacter* (early phase or epASV1) (61.0% and 58.3%, respectively) and *Muribacter* (epASV2) (14.0% and 9.0%, respectively) (Figure S4A). One additional taxon was prominent with LPS-induced intra-amniotic inflammation, *Staphylococcus* (epASV6) (3.5%), while two were prominent with sterile intra-amniotic inflammation, *Lactobacillus* (epASV4) (4.2%) and *Enterococcus* (epASV3) (3.8%) (Figure S4A). No effect on bacterial diversity was observed with progesterone action blockade (Figures 3H and 3I; Table S2). The prominent taxa observed in this group were *Rodentibacter*, *Muribacter*, and *Staphylococcus* (43.2%, 30.0%, and 4.3% for epASV1, epASV2, and epASV6, respectively) (Figure S4A). Notably, comparisons of the total number of ASVs observed in each group prior to labor and with SEL revealed a greater number of shared ASVs than of distinct ASVs regardless of stimulus, indicating that the vaginal microbiome in early stages of parturition is relatively unperturbed (Figures 3D, 3G, and 3J). No differences were found in bacterial diversity in the control groups (PBS or DMSO) with SEL (Figures S4A and S4C; Table S2).

With SAL, intra-amniotic LPS caused a reduction in bacterial richness (Figure 4B) as well as of variation in bacterial profile composition (Figure 4C; Table S3) and structure (Table S3). A similar but lesser effect was observed for intra-amniotic IL-1α (Figures 4E and 4F; Table S3), as indicated by the degree of variability in bacterial composition explained by each group (i.e., 18.6% of the variation in bacterial composition can be explained by LPS-induced intra-amniotic inflammation versus 11.4% due to sterile intra-amniotic inflammation). The taxonomic identities of the two most prominent (≥2% average relative abundance) ASVs for both LPS-induced and sterile intra-amniotic inflammation were *Rodentibacter* (active phase or apASV1) (54.1% and 52.1%, respectively) and *Muribacter* (apASV2) (19.9% and 26.5%, respectively) (Figure S4B). One additional prominent taxon, *Gemella*, was also shared (apASV5) (4.3% and 2.4%, respectively) (Figure S4B). The

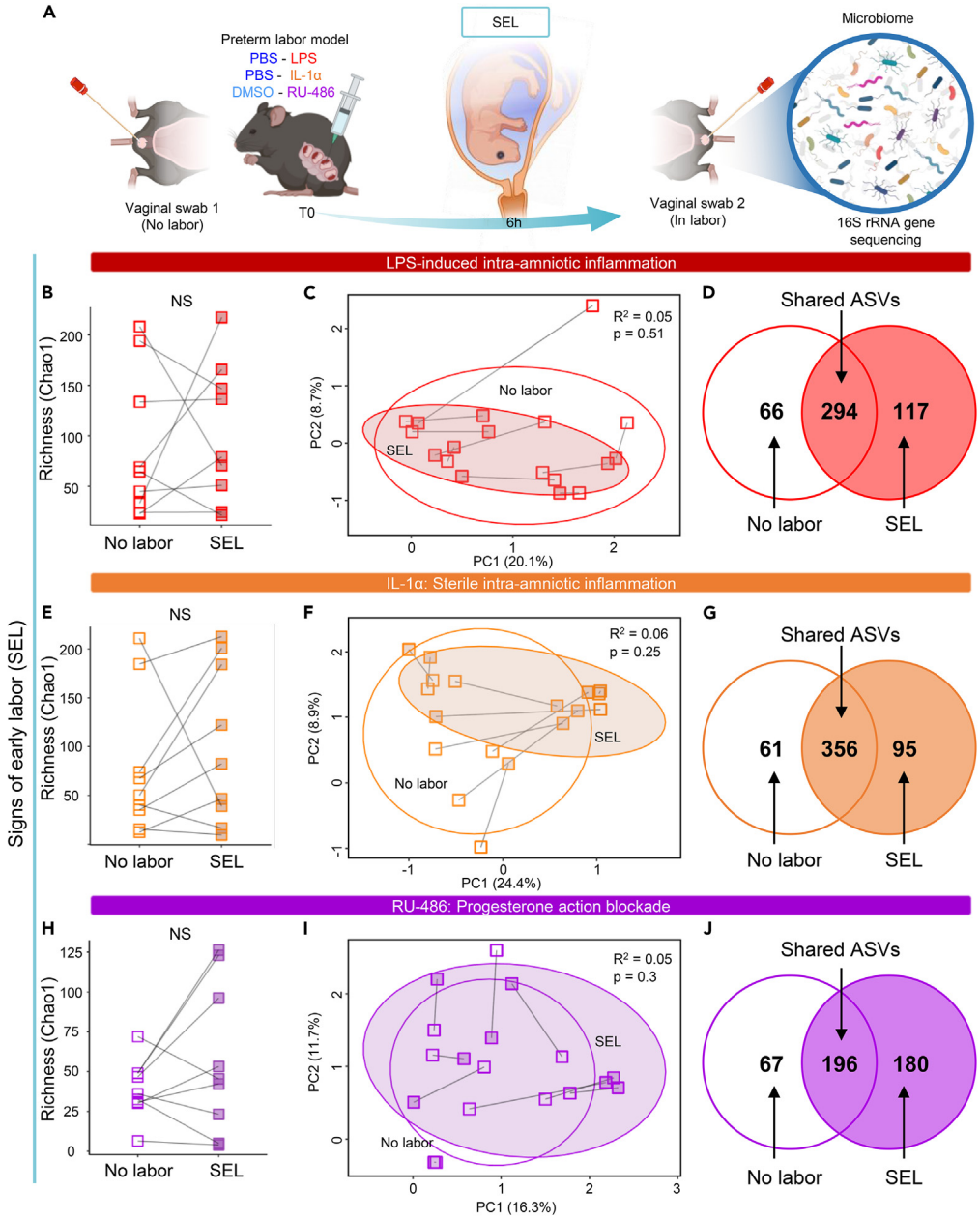

Figure 3. The vaginal microbiome does not change with signs of early premature labor

(A) An initial vaginal swab was collected without labor, prior to the administration of the stimulus to induce preterm labor (T0). Dams were then intra-amniotically injected with PBS, LPS, or IL-1α, or subcutaneously with DMSO or RU-486 (n = 6–9 dams per group), and a second vaginal swab was collected with signs of early premature labor (SEL; 6 h). The diversity of the vaginal microbiome was evaluated utilizing 16S rRNA gene sequencing data. Paired dot plots illustrate the richness of the vaginal microbiome accompanying SEL induced by (B) LPS, (E) IL-1α, or (H) RU-486. p values were determined by paired t-tests or Mann-Whitney U tests. Principal coordinate analysis plots (PCoA) of paired microbiome samples illustrate the composition accompanying SEL in dams with (C) LPS-induced intra-amniotic inflammation, (F) sterile intra-amniotic inflammation, or (I) progesterone action blockade. Ellipses indicate 80% confidence intervals. p values were determined by non-parametric multivariate analysis of variance (NPMANOVA) tests. Venn diagrams comparing bacterial taxa unique to or shared by the no labor and SEL states in dams with (D) LPS-induced intra-amniotic inflammation, (G) sterile intra-amniotic inflammation, or (J) progesterone action blockade. Each group is color-coded with open symbols representing no labor and filled symbols representing SEL. NS, non-significant. See also Figures S4 and S5 and Table S2.

vaginal microbiome in LPS-induced intra-amniotic inflammation included two prominent *Streptococcus* (apASV3 and apASV4) (8.5% and 5.8%), while that of sterile intra-amniotic inflammation had a prominent presence of *Staphylococcus* (apASV10) (3.8%) (Figure S4B). No effect on bacterial diversity was observed after progesterone action blockade (Figures 4H and 4I; Table S3). Prominent taxa in this group included

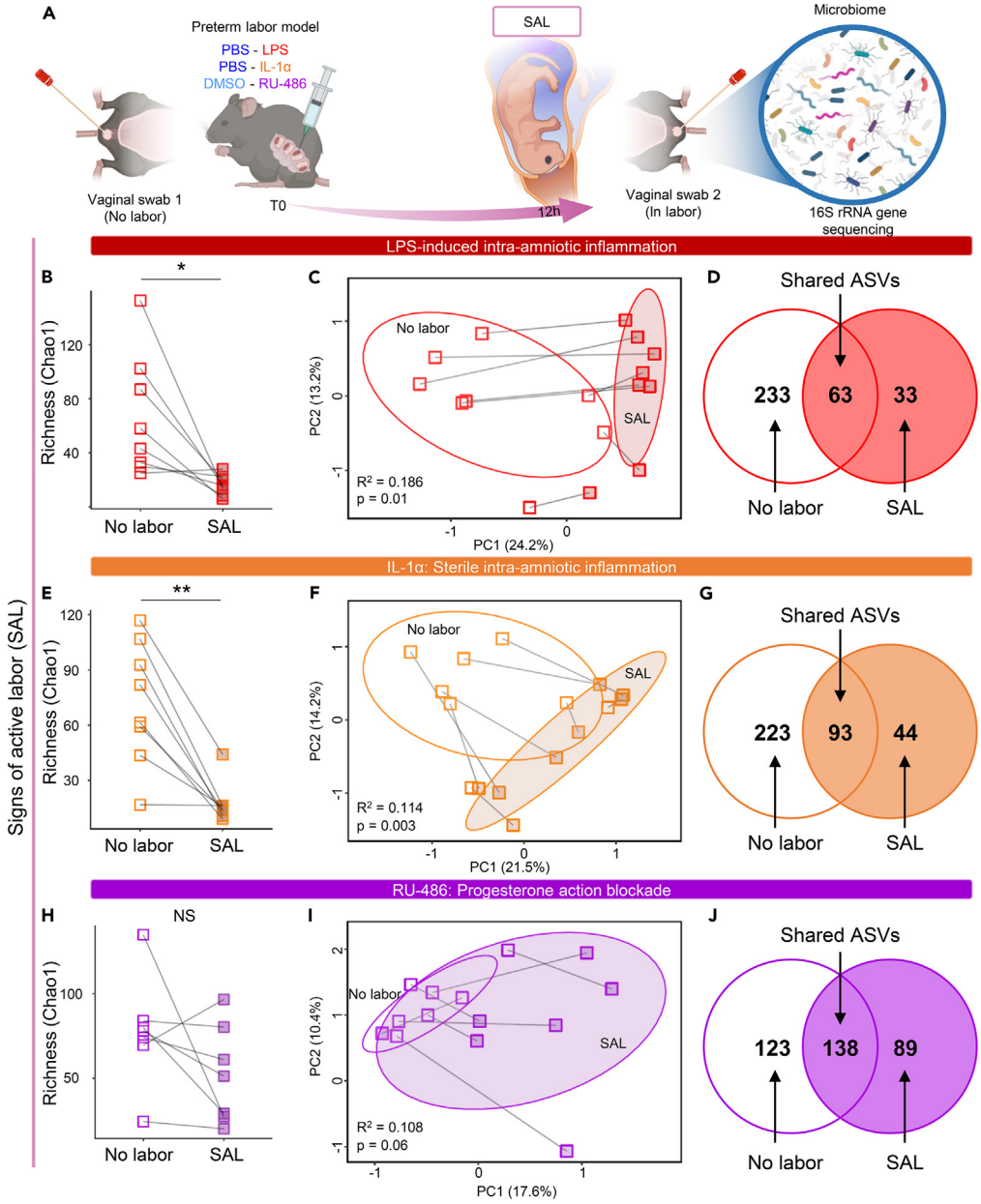

Figure 4. The vaginal microbiome changes with signs of active premature labor solely in the presence of intra-amniotic inflammation

(A) An initial vaginal swab was collected without labor, prior to the administration of the stimulus to induce preterm labor (T0). Dams were then intra-amniotically injected with PBS, LPS, or IL-1α, or subcutaneously with DMSO or RU-486 (n = 6–9 dams per group), and a second vaginal swab was collected with signs of active premature labor (SAL; 12 h). The diversity of the vaginal microbiome was evaluated utilizing 16S rRNA gene sequencing data. Paired dot plots illustrate the richness of the vaginal microbiome with SAL induced by (B) LPS, (E) IL-1α, or (H) RU-486. p values were determined by paired t tests or Mann-Whitney U tests. Principal coordinate analysis plots (PCoA) of paired microbiome samples illustrate the shift in composition accompanying SAL in dams with (C) LPS-induced intra-amniotic inflammation, (F) sterile intra-amniotic inflammation, or (I) progesterone action blockade. Ellipses indicate 80% confidence intervals. p values were determined by non-parametric multivariate analysis of variance (NPMANOVA) tests. Venn diagrams comparing bacterial taxa unique to or shared by the no labor and SAL states in dams with (D) LPS-induced intra-amniotic inflammation, (G) sterile intra-amniotic inflammation, or (J) progesterone action blockade. Each group is color-coded with open symbols representing no labor and filled symbols representing SAL. *p < 0.05; **p < 0.01. NS, non-significant. See also Figures S4 and S5 and Table S3.

Rodentibacter (apASV1), *Muribacter* (apASV2), *Gemella* (apASV5), and *Streptococcus* (apASV3 and apASV4) (at 68.2%, 13.8%, 4.6%, 3.4%, and 2.8%, respectively) (Figure S4B), which were also observed in LPS- and IL-1α-injected dams. Additionally, when assessing the total observed ASVs in each group, we observed a dramatic reduction in ASVs between the initial time point and SAL induced by intra-amniotic LPS and IL-1α

(Figures 4D and 4G) but not upon RU-486 injection (Figure 4J). No differences in bacterial diversity were found in the control groups (PBS or DMSO) with SAL (Figures S4B and S4D; Table S3). As evidence that the microbiome changes were driven by the process of active labor, we confirmed that there were no differences in alpha or beta diversity of the vaginal microbiome at pre-labor sampling among the study groups (Figures S4E and S4F).

Altogether, these data suggest that LPS-induced intra-amniotic inflammation and sterile intra-amniotic inflammation can lead to alterations in the vaginal microbiome that manifest together with signs of active premature labor but are not apparent with signs of early premature labor. These variations did not result in a significant change in the prominent bacterial taxa in the vaginal microbiome, suggesting that the selective pressures from the intra-amniotic inflammatory response are likely influencing or more effectively eliminating the rare or lower abundance in members of the microbiome. Therefore, linear discriminant analysis effect size (LEfSe) was used to further evaluate the differences in relative abundances of bacterial taxa at broader taxonomic scales (i.e., Family and Genus-level, as opposed to ASV-level changes) within the vaginal microbiome between SEL and SAL for each respective study group. The differences in taxonomic features between no labor and SEL were limited to only a few taxa for each group (Figures S5A–S5C). Notably, despite the previously observed variation in bacterial diversity for both intra-amniotic LPS and intra-amniotic IL-1α with SAL (Figures 4B, 4C, 4E, and 4F), a robust group of taxonomic features was identified as more relatively abundant before labor than with SAL exclusively in LPS-induced intra-amniotic inflammation (Figure S5D). This observation is in stark contrast with the greatly limited number of features identified in sterile intra-amniotic inflammation and progesterone action blockade (Figures S5E and S5F). These data support the concept that LPS-induced intra-amniotic inflammation drives a more substantive response toward the vaginal microbiome than sterile intra-amniotic inflammation, affecting a wide range of bacterial taxa yet leaving the prominent members relatively unaltered. The fact that RU-486 injection did not result in alterations in the vaginal microbiome with signs of early and active premature labor indicates that not all preterm birth subsets are consistently preceded by changes in the vaginal microenvironment.

Local immune responses in the cervix and vagina occur with signs of early premature labor and active premature labor

Up to this point, we have shown that LPS, IL-1α, and RU-486 induce stereotypic intra-amniotic inflammatory responses with SEL and SAL and that the vaginal microbiome changes after the onset of preterm parturition in the presence of intra-amniotic inflammation. Changes in the vaginal microbiome are intertwined with local immune responses[41–43,46,67–69]; therefore, we next investigated the inflammatory responses in the cervicovaginal space with SEL or SAL. To address this research question, the cervix was collected in early premature labor, and histologic techniques (Movat pentachrome, immunohistochemistry, and immunofluorescence) were performed to evaluate tissue structure as well as leukocyte infiltration and identity (Figure 5A, STAR Methods). The intra-amniotic administration of LPS or IL-1α resulted in increased mucin (green/blue stain) production by cervical epithelial cells compared to controls with SEL (Figure 5B). Such changes in the cervical epithelium were not evident after RU-486 injection (Figure 5B). Furthermore, leukocyte infiltration was enhanced in the cervixes of dams injected with LPS and IL-1α with SEL (Figures 5C–5E). Such an increase did not reach statistical significance after injection with RU-486 (Figures 5C and 5F). Multiplex immunofluorescence revealed that the predominant immune cells infiltrating the cervix with SEL were neutrophils and macrophages, regardless of the stimuli (Figures 5G–5I). Next, we evaluated the same parameters with SAL. Although no structural changes were evident between LPS-, IL-1α-, or RU-486-injected and their respective controls (data not shown), a greater infiltration of immune cells, mainly neutrophils and macrophages, was observed with SAL in all three models (Figure S6A–S6G). These data show that cellular immune responses occur in the cervix with signs of early and active premature labor in the context of LPS-induced and sterile intra-amniotic inflammation, yet such an immune response can be a consequence of the onset of labor triggered by progesterone action blockade.

Next, we evaluated whether leukocyte infiltration in the cervix was accompanied by changes in expression of transcripts related to immune response,[70–72] contractility,[73] collagen degradation,[72,74–76] and structural functions.[77–80] Cervical changes are likely to be synchronized with those occurring in the vagina,[81,82] the niche for the microbial communities that could potentially invade the cervix and ultimately reach the amniotic cavity[31,83]; therefore, we also determined gene expression in the vagina. The cervix and vagina were collected with SEL or SAL to perform targeted RT-qPCR (Figures 6A and S7A STAR Methods). Intra-amniotic injection of LPS induced inflammatory responses in the cervix accompanying SEL or SAL; yet, such responses were distinct (Figures 6B and S7B). With SEL, the expression of *Nfkb1*, *Nfkb2*, *Tnf*, *Cxcl1*, *Cxcl5*, and *Tlr4* was greater upon LPS injection compared to PBS-injected controls (Figure S7B), but these transcripts were not increased in the active phase (Figure 6B). Moreover, the expression of *Adamts1*, *Camp*, *Ccl2*, *Has1*, *Lox*, *Mmp8*, *Slpi*, *Thbs2*, and *Tnc* was increased with SAL induced by LPS (Figure 6B), but such genes were not altered with SEL (Figure S7B). The intra-amniotic injection of IL-1α induced a milder inflammatory response in the cervix than LPS; however, it was also distinct between SEL and SAL (Figures 6C and S7C). While the cervical expression of *Cxcl1*, *Nfkb2*, and *Casp11* was increased only with SEL, an overexpression of *Adamts1*, *Camp*, *Mmp8*, *Mmp9*, and *Oxtr* was solely observed with SAL in the IL-1α model (Figures 6C and S7C). The administration of RU-486 induced a mild inflammatory response in the cervix with SEL showing decreased expression of *Cxcl10* and *Tlr4*, which were not altered with SAL (Figures 6D and S7D). Notably, a massive transcriptomic response was observed in the cervix with SAL in the RU-486 model, with an increased expression of *Ccl2*, *Cldn4*, *Il6*, *Krt8*, *Lox*, *Mmp8*, *Nlrp3*, *Oxtr*, *Ptgs2*, *Thbs1*, and *Tnc*, as well as a reduced expression of *Casp1*, *Casp11*, *Col3a1*, *Dcn*, *Defb1*, *Has2*, *Il18*, *Lum*, and *Mmp9*, which were not altered with SEL (Figures 6D and S7D). It is worth mentioning that the expression of *Oxtr* and *Gja1* (i.e., key molecules for cervical contractility[73]) in the cervix was increased with SAL in all three study groups compared to controls (Figures 6B–6D), providing molecular evidence of the ongoing parturition cascade.

Gene expression profiles in the vagina were also altered with SEL and SAL. Specifically, with SEL, the vaginal expression of *Has2* was increased but that of *Il1b*, *Thbs1*, and *Cxcr2* was reduced upon LPS administration compared to controls (Figure S7E). None of these transcripts were altered with SAL (Figure 6E). Moreover, the vaginal expression of *Camp*, *Casp11*, *Ccl2*, *Cxcl1*, *Gja1*, *Il6*, *Lox*, *Mmp8*, *Nfkb2*,

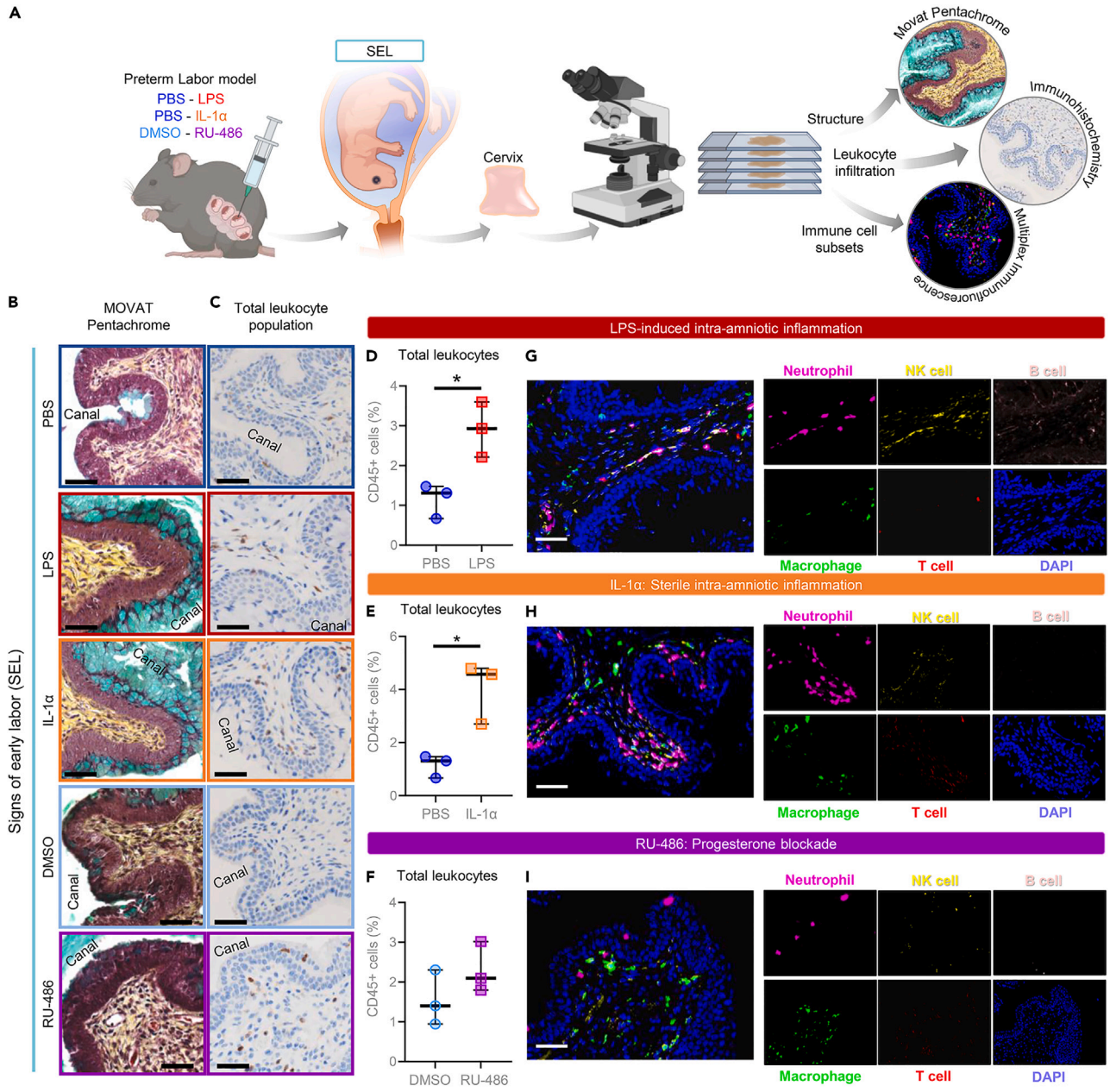

Figure 5. Local immune responses in the cervix with signs of early premature labor or active premature labor

(A) Dams were intra-amniotically injected under ultrasound guidance with PBS, LPS, or IL-1α, or subcutaneously with DMSO or RU-486 (n = 3 dams per group). The cervix was collected with signs of early premature labor (SEL; 6 h) and histology was utilized to evaluate structure by Movat pentachrome staining, leukocyte infiltration by immunohistochemistry, and leukocyte subsets by multiplex immunofluorescence.

(B) Representative Movat pentachrome staining images of the cervix from control (PBS and DMSO) and preterm labor (LPS, IL-1α, and RU-486) mice with SEL. Blue staining indicates mucin, yellow indicates collagen, and red/bright red indicates muscle/fibrin. Nuclei appear as dark blue/black.

(C) Representative images showing 3,3′diaminobenzidine (DAB) immunohistochemistry to detect the pan-leukocyte marker CD45 in the cervix of control (PBS and DMSO) and premature labor (LPS, IL-1α, and RU-486) mice (n = 3 per group) with SEL.

(D–F) Semi-quantification of the percentage of $CD45^+$ cells among all cells for each study group comparison. Data are shown as dot plots where midlines indicate medians and whiskers indicate minimum and maximum values. p values for the comparisons between groups were determined by unpaired t tests. *$p < 0.05$.

(G–I) Representative merged images showing the co-localized immunofluorescence detection of neutrophils ($Ly6G^+$ cells, pink), monocytes/macrophages ($F4/80^+$ cells, green), T cells ($CD3^+$ cells, red), B cells ($CD19^+$ cells, light pink), and NK cells ($NCR1^+$ cells, yellow) in the cervices of treated mice (LPS, IL-1α, and RU-486) (n = 3 per group) with SEL. Nuclear staining is shown in blue (4′,6-diamidino-2-phenylindole; DAPI). Images were taken at 20X magnification. Scale bars represent 50μm. See also Figure S6.

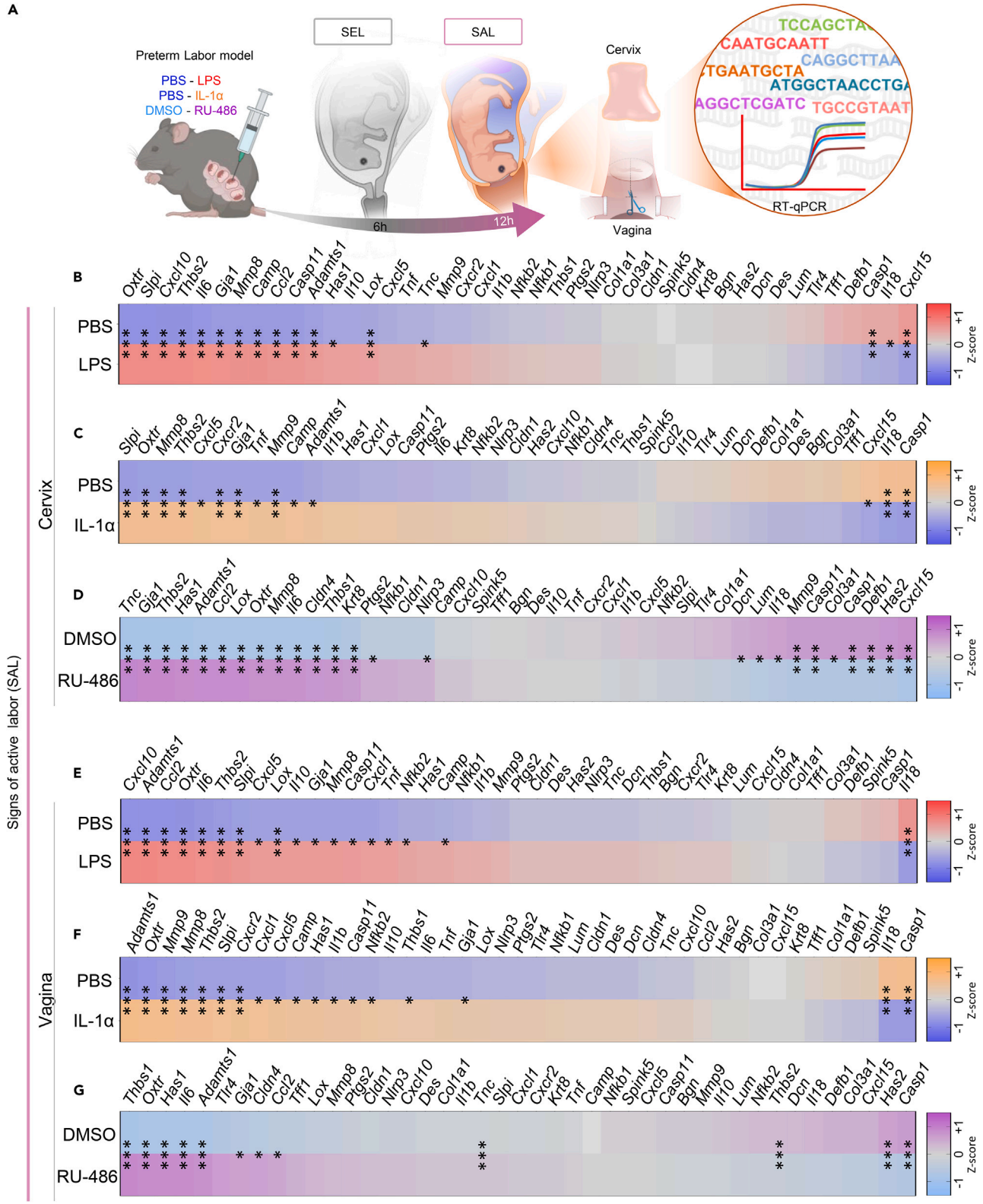
A
Preterm Labor model
PBS - LPS
PBS - IL-1α
DMSO - RU-486
SEL
SAL
6h
12h
Cervix
Vagina
RT-qPCR
Signs of active labor (SAL)
Cervix
Vagina
PBS
LPS
IL-1α
DMSO
RU-486
Z-score

Figure 6. Local immune responses in the cervix and vagina with signs of early premature labor or active premature labor

(A) Dams were intra-amniotically injected under ultrasound guidance with PBS, LPS, or IL-1α, or subcutaneously with DMSO or RU-486 (n = 9–10 dams per group). The cervix and vagina were collected with signs of early premature labor (SEL; 6h) or signs of active premature labor (SAL; 12 h), and targeted RT-qPCR was utilized to assess gene expression. Heatmap representations showing differential gene expression ($-\Delta C_T$) in the cervices of dams injected with (B) PBS or LPS, (C) PBS or IL-1α, and (D) DMSO or RU-486 with SAL. Heatmap representations showing differential gene expression ($-\Delta C_T$) in the vagina of dams injected with (E) PBS or LPS, (F) PBS or IL-1α, and (G) DMSO or RU-486 with SAL. Heatmaps represent the mean of the *Z*-score of $-\Delta C_T$. p values were determined by Mann-Whitney U tests. *p < 0.05; ***p < 0.001. See also Figure S7.

Slpi, and *Tnf* was increased with SAL induced by LPS (Figure 6E), but such genes were not altered with SEL (Figure S7E). The intra-amniotic injection of IL-1α induced a minimal response in the vagina accompanying SEL, with *Cxcl10* being exclusively increased with SEL but not with SAL (Figures 6F and S7F). Yet, intra-amniotic IL-1α resulted in the upregulated expression of *Adamts1*, *Camp*, *Casp11*, *Cxcl1*, *Cxcl5*, *Cxcr2*, *Gja1*, *Has1*, *Il1b*, *Mmp8*, *Mmp9*, *Nfkb2*, *Oxtr*, *Slpi*, *Thbs1*, and *Thbs2* in the vagina with SAL (Figure 6F). RU-486 induced a mild response in the vagina with SEL, showing a decreased expression of *Cldn1* that was not altered with SAL (Figures 6G and S7G). The vaginal gene expression profile was greater with SAL than with SEL, showing an overexpression of *Ccl2*, *Cldn4*, *Gja1*, *Il6*, and *Tnc* and downregulation of *Casp1* (Figure 6G). Last, the vaginal expression of *Oxtr*, *Gja1*, and *Adamts1* was increased with SAL among all three preterm birth models (Figures 6E–6G).

Collectively, these results indicate that changes in cervical and vaginal transcriptomic activity are evident, but modest, with signs of early premature labor, regardless of the nature of the labor-inducing stimulus; however, such gene expression is enhanced with signs of active premature labor after the establishment of parturition.

LPS, IL-1α, and RU-486 facilitate bacterial ascension into the amniotic cavity, resulting in preterm birth

The aforementioned findings showed that cervico-vaginal processes, including inflammation, are evident with SEL regardless of the stimuli. Previous research has shown a heightened occurrence of intra-amniotic infection and histologic chorioamnionitis in women undergoing active labor compared to those not in labor at term.[84,85] Therefore, we reasoned that the onset of labor, which occurs before observing signs of early labor,[53,86–88] could facilitate the ascension of microbes from the lower genital tract into the amniotic cavity (Figure 7A). To test this hypothesis, pregnant mice received the stimuli to induce preterm birth or the respective vehicle control, and immediately afterward (i.e., in the absence of cervical shortening) underwent the ultrasound-guided vaginal inoculation of GFP-expressing *E. coli* (*E. coli* GFP) (Figure 7B, STAR Methods). Bacterial ascension, as evidenced by the detection of the GFP signal in the uterine tissues and amniotic fluid, was assessed at 2–3 h and 6–8 h post-inoculation (Figure 7B), given that mice receiving LPS, IL-1α, or RU-486 followed by bacterial inoculation delivered preterm neonates within 10–12 h (data not shown). Bacterial ascension was evident at 6–8 h post-inoculation in dams injected with LPS, IL-1α, or RU-486 (Figure 7C) together with signs of labor (data not shown). Yet, the GFP signal was not observed in control dams injected with PBS or DMSO (Figure 7C) or in background controls that received intra-vaginal PBS (data not shown). The magnitude and localization of the fluorescent signal are shown by 3D representations in dams undergoing bacterial ascension and in controls (Figure 7D). We confirmed that the fluorescence signal detected transabdominally was indeed emitted by the intra-uterine compartment, as evidenced by the representative images shown in Figure 7E. Importantly, the GFP signal was also observed in the amniotic fluid (Figure 7F). Indeed, the amniotic fluid GFP signal was detected in 100% of dams with LPS-induced intra-amniotic inflammation (Figure 7G), in 80% of dams with sterile intra-amniotic inflammation (Figure 7H), and in 60% of the dams with progesterone action blockade (Figure 7I). Hence, preterm labor induced by microbial products, alarmins, or progesterone action blockade facilitates the ascension of bacteria from the lower genital tract into the amniotic cavity.

DISCUSSION

Investigations of the vaginal microbiome during gestation revealed a delicate interplay between the host and commensal microbes that is essential for a healthy pregnancy.[81,89–92] Disruptions of this balance have been linked to preterm birth[41–44,46,93]; however, detecting changes in the vaginal microbiome as a reliable, clinically relevant biomarker for preterm birth remains challenging.[47] Herein, we demonstrated that the vaginal microbiome is altered only with signs of active premature labor induced by intra-amniotic LPS or IL-1α, but not by progesterone action blockade, indicating that not all preterm births are preceded by changes in the vaginal microbiome. These results may provide an explanation as to why the sole consideration of the vaginal microbiome, but not other factors implicated in the host response, is generally insufficient to be used as a biomarker for preterm birth. Indeed, our group is part of a multidisciplinary team that has recently undertaken a longitudinal investigation to study the vaginal microbiome[48] and the vaginal immunoproteome[49] in spontaneous preterm birth cases (preterm labor with intact membranes or PPROM). We found that the predictability of premature birth using either the vaginal microbiome or the immunoproteome varies according to the preterm birth subset, with the vaginal immunoproteome being the best predictor of early PPROM (i.e., delivery <34 weeks),[49] a subset of preterm births with a high rate of adverse perinatal outcomes.[94,95] Similarly, the vaginal microbiome was a better predictor of early PPROM than other preterm birth subsets[48]; yet, such predictive power was not superior to that of the vaginal immunoproteome.[49] Hence, we are currently investigating whether a comprehensive approach that combines the study of the vaginal microbiome through metagenomics and the vaginal immunoproteome can provide better insights into the host-microbiome interactions in the cervico-vaginal niche in the context of spontaneous preterm birth. We hypothesize that this combined approach will enhance the power to predict spontaneous preterm births, as compared to studying each component separately.

We also showed herein that the alteration of the vaginal microbiome induced by intra-amniotic LPS or IL-1α together with signs of active premature labor included a reduction in bacterial richness and variation in the bacterial profile composition, which did not significantly affect

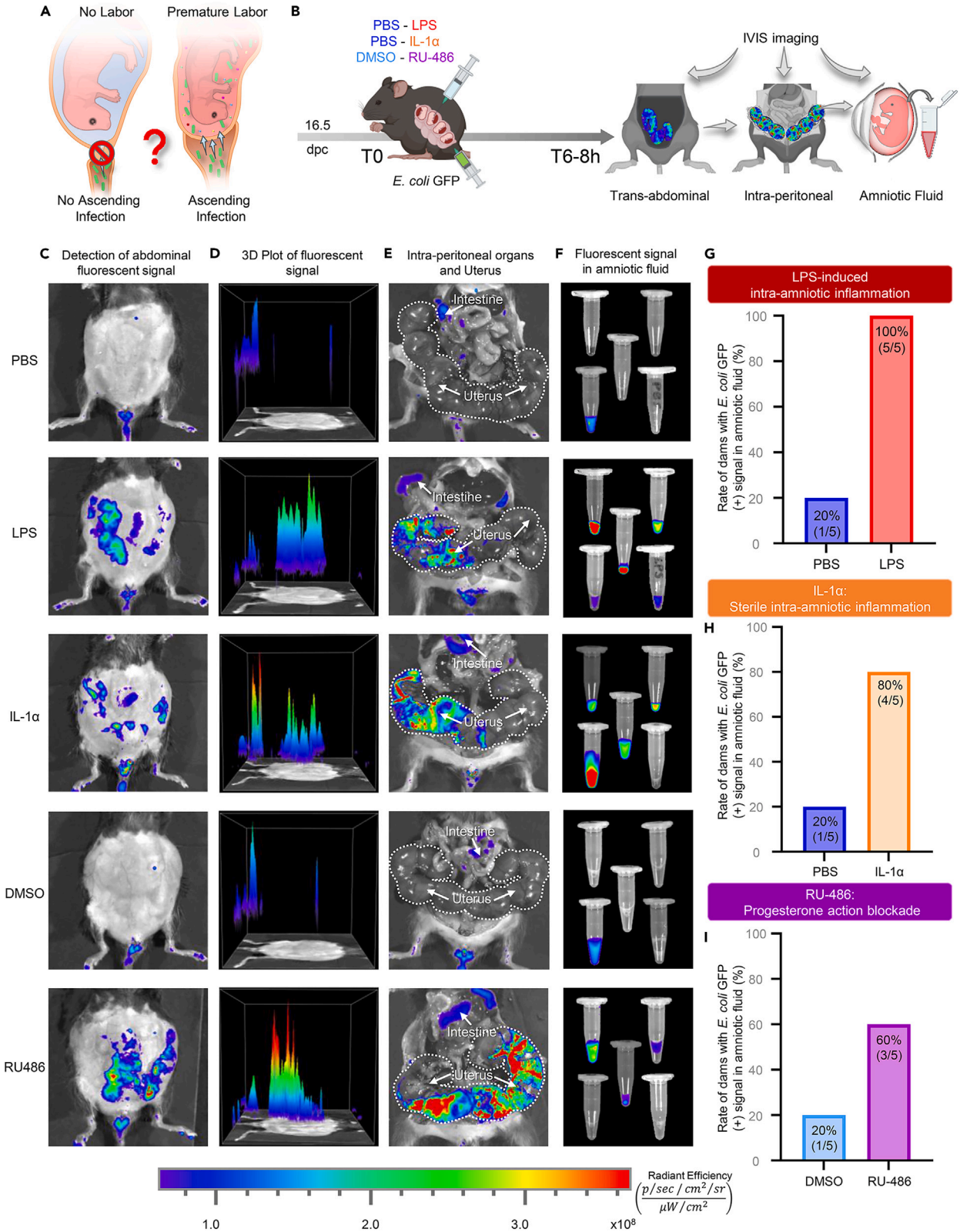
A
No Labor
Premature Labor
No Ascending Infection
Ascending Infection
B
PBS - LPS
PBS - IL-1α
DMSO - RU-486
16.5 dpc
T0
E. coli GFP
T6-8h
IVIS imaging
Trans-abdominal
Intra-peritoneal
Amniotic Fluid
C Detection of abdominal fluorescent signal
D 3D Plot of fluorescent signal
E Intra-peritoneal organs and Uterus
F Fluorescent signal in amniotic fluid
PBS
LPS
IL-1α
DMSO
RU486
Intestine
Uterus
1.0
2.0
3.0
x10⁸
Radiant Efficiency
(p/sec/cm²/sr)/(μW/cm²)
G
LPS-induced intra-amniotic inflammation
Rate of dams with E. coli GFP (+) signal in amniotic fluid (%)
100%
(5/5)
20%
(1/5)
PBS
LPS
IL-1α:
Sterile intra-amniotic inflammation
H
80%
(4/5)
20%
(1/5)
PBS
IL-1α
RU-486:
Progesterone action blockade
I
60%
(3/5)
20%
(1/5)
DMSO
RU-486

Figure 7. LPS, IL-1α, and RU-486 facilitate bacterial ascension into the amniotic cavity resulting in preterm birth

(A) We hypothesized that preterm labor would facilitate the ascension of bacteria from the vagina into the intra-amniotic space, a phenomenon that would be limited in the absence of preterm labor.

(B) Dams were intra-amniotically injected under ultrasound guidance with PBS, LPS, or IL-1α, or subcutaneously with DMSO or RU-486 (n = 5 dams per group). Immediately after the injection of the stimuli, GFP-expressing *Escherichia coli* (*E. coli* GFP) were inoculated in the cervico-vaginal space next to the external limit of the cervix under ultrasound guidance (T0). Six-to-eight h later, IVIS imaging of the abdomen, peritoneal cavity, and amniotic fluid was performed to detect bacterial ascension.

(C) Representative images showing the detection of the bacteria in the abdomen of dams from each study group.

(D) Representative 3D plots showing the distribution and magnitude of the fluorescent signal detected in dams among the study groups.

(E) Representative images of the intra-peritoneal organs and the uterus showing the localization of the fluorescence signals within the abdominal cavity.

(F) Amniotic fluid collected from dams showing the fluorescent signal detected by IVIS imaging in each study group. Bar plots showing the rate of positive fluorescence signal detection in the amniotic fluid of dams injected with (G) PBS or LPS, (H) PBS or IL-1α, and (I) DMSO or RU-486. All fluorescence images were adjusted to the same scale shown at the bottom of the figure.

the most prominent bacterial taxa in the vaginal microbiome. These results indicate that the intra-amniotic inflammatory response is influencing those members of the vaginal microbiome with lower relative abundance. Notably, the vaginal microbiome in the vehicle control groups sampled at 0 and 6h, or at 0 and 12 h, was not altered following the repeated swabbing, suggesting that temporally separated swabs do not affect the diversity of the vaginal microbiome. A previous human study showed that women with spontaneous premature labor and intra-amniotic inflammation displayed higher diversity in their vaginal microbiome but without differences in richness.[96] Moreover, amniotic fluid concentrations of IL-6 were inversely correlated with the bacterial load of *Lactobacillus* spp. in the vaginal fluid of women with spontaneous premature labor and intra-amniotic inflammation.[96] These results are in line with our findings of an altered vaginal microbiome only in the context of preterm labor with intra-amniotic inflammation. Yet, the specific mechanisms whereby only some specific cervico-vaginal bacterial taxa are affected by intra-amniotic inflammation require further investigation. Furthermore, prior studies have documented that alterations in other murine niches, such as the gut microbiome, can be detected as early as 4–6 h.[97,98] Therefore, this evidence supports our current data by showing that mice are indeed susceptible to rapid detectable changes in their microbiome.

The current study utilized three different murine models of preterm birth to demonstrate that each stimulus drives different underlying mechanisms of disease. While the intra-amniotic injection of LPS induced a massive inflammatory response in the amniotic cavity, the response induced by IL-1α was milder. Moreover, these intra-amniotic inflammatory responses were distinct between signs of early and active premature labor. Such differences could be attributed not only to the stage of labor but also to the intrinsic kinetics triggered by the different inflammatory stimuli; yet, the latter concept requires further experimentation with a time course for each specific model of preterm labor and birth. Previous investigations by our group have shown that the amniotic fluid concentrations of immune mediators are different and greater in women with microbial intra-amniotic inflammation than in those with sterile intra-amniotic inflammation,[60,61] although both entities result in similar clinical outcomes.[36] Furthermore, using RNA-sequencing, we previously showed that the chorioamniotic membranes of women with microbial intra-amniotic inflammation display distinct transcriptomic profiles from those with sterile intra-amniotic inflammation.[99] Indeed, the immune response in the chorioamniotic membranes of women with sterile intra-amniotic inflammation was milder than that induced by microbes and involved the upregulation of alarmins.[99] Nonetheless, the results of our current investigation, together with animal studies wherein the administration of microbes[10,12,19,23,25,100] or alarmins[13,18,20–22,101–103] in the amniotic cavity induced premature labor and birth, indicate that the microbial product- or alarmin-induced intra-amniotic inflammatory response can be a cause of labor.

Herein, we also report that RU-486 induced only a mild intra-amniotic inflammatory response accompanying signs of active premature labor. This finding is consistent with a study using the progesterone action blockade model of preterm birth that showed no increase in inflammatory mediators in the amniotic fluid or in the fetal brain during early phases of premature labor (i.e., 6 h after administration of RU-486).[104] Moreover, we previously showed that RU-486 induces preterm labor accompanied only by increased amniotic fluid concentrations of IL-23 and a tendency for increased IL-6 in more advanced premature labor (i.e., 12–16 h after administration of RU-486).[40] These results are in line with our current findings and demonstrate that, in the clinical scenario wherein preterm birth is caused by progesterone deficiency, intra-amniotic inflammation is a consequence of the process of labor rather than a cause.

In the current study, we investigated the local inflammatory response induced by different stimuli in the cervico-vaginal microenvironment and demonstrated an inflammatory milieu that increased from signs of early premature labor to signs of active premature labor. Our data are in line with previous transcriptomic studies of the cervix at term, which together provided the following evidence for a continuum of increasing inflammation prior to and during labor: (1) modulation of biological processes related to structural changes, but not inflammation, was reported during ripening prior to labor[105]; (2) upregulation of immunological processes takes place during shortening prior to labor[106]; and (3) inflammatory processes occur in tandem with dilatation in women with labor at term.[107] The immune cellular infiltration in the cervical tissues during the process of labor has been previously demonstrated to be predominantly driven by innate immune cells,[108–117] which is consistent with the findings presented herein. Moreover, we recently used single-cell RNA sequencing to reveal that premature labor induced by the intra-amniotic inoculation of *E. coli* also induces the cervical infiltration of neutrophils together with transcriptomic alterations in innate immune cells and epithelial cells.[25] Here, we showed for the first time that sterile intra-amniotic inflammation induces immune and structural changes in the cervico-vaginal space. Furthermore, while local inflammation is observed with signs of early and active premature labor, alteration of the cervico-vaginal microbiome is found only at the latter time point, suggesting that the cervical immune response precedes and shapes changes to the microbiome prior to premature birth. This finding may have clinical implications and can potentially explain why the evaluation of the vaginal microbiome alone has not been successful for the prediction of premature labor and preterm birth. It is worth

mentioning that an inflammatory response during premature labor was also observed in the vaginal tissues, the role of which during labor has been largely under-investigated.

Multiple routes for microbial invasion of the amniotic cavity have been proposed, such as the ascension of microbes from the lower genital tract through the cervix, hematogenous dissemination, retrograde invasion from the peritoneal cavity through the fallopian tubes, and accidental introduction of microbes during an invasive procedure (e.g., amniocentesis).[8,9,31,118,119] We recently demonstrated that ascending invasion is the primary route by which microbes access the amniotic cavity in humans, as evidenced by the high degree of similarity between bacterial profiles from the vaginal fluid and amniotic fluid of the same pregnant women.[31] In line with this concept, animal models have shown that the intra-cervical or intra-vaginal inoculation of bacteria can induce preterm birth via an ascending mechanism.[71,120–124] Chemical agents[122] or microbes[67,69,76,125–127] in the cervico-vaginal space may cause epithelial damage, which could then promote the ascension of bacteria leading to preterm birth. Moreover, mice lacking a key gene for epithelial integrity, *Has2*, experience high rates of preterm birth upon intra-vaginal inoculation of *E. coli*,[71] suggesting that disruption of local defense mechanisms can encourage bacterial ascension. Alternatively, in the current study, we show that the inflammatory milieu in the amniotic cavity induced by LPS or IL-1α can perturb the gene expression of key molecules related to structure and contractility in the cervix, which may also facilitate bacterial ascension. Our results are in line with previous investigations demonstrating structural and transcriptomic changes in the cervix after the intra-uterine injection of LPS.[70,72,128–130] Indeed, using our model of intra-amniotic *E. coli*-induced premature labor and birth, we showed that the biological processes enriched in epithelial cells and infiltrating innate immune cells in the cervix were associated with anti-bacterial immune responses.[25] Moreover, cell-cell signaling pathways related to extracellular matrix were strongly represented in the murine cervix from dams undergoing premature labor induced by intra-amniotic inoculation of *E. coli*.[25] Thus, microbial intra-amniotic inflammation can alter cellular functionality in the cervix, which may ultimately promote bacterial ascension. Finally, herein we demonstrated for the first time that the premature process of labor itself, regardless of the specific stimuli, facilitated the ascension of bacteria from the vagina into the amniotic cavity. Although the exact mechanisms that allow such ascension were not elucidated in the current study, our results support human data demonstrating that uterine contractions can exert a "suction-like effect",[131] which could introduce microbes from the vagina into the amniotic cavity and trigger a local acute inflammatory response in the active phase of labor, as supported by the higher rates of microbial invasion of the amniotic cavity and histologic chorioamnionitis in women with active labor compared to those in the latent phase of labor or those without labor at term.[84,85] Yet, such processes had not been investigated during premature labor.

Collectively, this study reveals the interplay between the host and microbiome in the cervico-vaginal microenvironment across three distinct subsets of preterm labor and birth: LPS-induced intra-amniotic inflammation, sterile intra-amniotic inflammation, and progesterone action blockade. First, we demonstrated that intra-amniotic LPS triggers inflammatory responses in the amniotic cavity and cervico-vaginal space that differ between signs of early and active premature labor, leading to alteration of the vaginal microbiome and impending delivery. Intra-amniotic delivery of IL-1α induced a moderate inflammatory response in the amniotic cavity and cervico-vaginal tissues that differs between signs of early and active labor, causing a disruption of the vaginal microbiome accompanying signs of active premature labor prior to preterm birth. Conversely, progesterone action blockade by RU-486 only induced intra-amniotic inflammation and triggered increasing inflammatory responses in the cervico-vaginal microenvironment with signs of active premature labor but did not alter the vaginal microbiome. Notably, preterm labor induced by any of the three stimuli facilitated the ascension of bacteria into the amniotic cavity. Taken together, our findings have uncovered compelling mechanistic insights into the dynamic host-microbiome interactions within the cervico-vaginal microenvironment, which are implicated in the onset of premature labor. This newfound understanding has the potential to significantly advance the development of non-invasive biomarkers for preterm birth, ultimately improving clinical outcomes for expectant mothers and their newborns.

LIMITATIONS OF THE STUDY

Our study is not exempt from some limitations. First, the diagnosis of labor in humans is based on clinical signs of uterine contractions and cervical modifications evaluated by digital examination. However, given that digital examination is not feasible in mice, the sonographic findings of cervical shortening and uterine contraction-like movements in tandem with the molecular signatures of labor (e.g., upregulation of contractility-associated genes) strongly support our diagnosis of labor in mice. Moreover, while the latent (i.e., early) and active phases of labor have been characterized in human parturition at term, they have not been described in premature labor.[132–135] Therefore, due to the lack of nomenclature and description of these phases in premature labor in humans or mice, we referred to them as "signs of early premature labor" and "signs of active premature labor." Lastly, the ascension of bacteria was determined based on fluorescent signals, and bacteria quantification or viability was not assessed. Yet, the dramatic differences observed between the preterm labor and vehicle control groups were sufficient to demonstrate that premature labor facilitates the ascension of bacteria. Therefore, whether the premature labor-facilitated ascending bacteria are viable and capable of causing harm *in utero* requires further investigation.

STAR★METHODS

Detailed methods are provided in the online version of this paper and include the following:

- KEY RESOURCES TABLE
- RESOURCE AVAILABILITY
  - Lead contact
  - Materials availability

SUPPLEMENTAL INFORMATION

Supplemental information can be found online at https://doi.org/10.1016/j.isci.2023.108341.

ACKNOWLEDGMENTS

This research was supported by the Perinatology Research Branch, Division of Obstetrics and Maternal-Fetal Medicine, Division of Intramural Research, *Eunice Kennedy Shriver* National Institute of Child Health and Human Development, National Institutes of Health, U.S. Department of Health and Human Services (NICHD/NIH/DHHS) under Contract No. HHSN275201300006C. This research was also supported by the Wayne State University Perinatal Initiative in Maternal, Perinatal and Child Health. R.R. has contributed to this work as part of his official duties as an employee of the United States Federal Government. The funders had no role in study design, data collection and interpretation, or the decision to submit the work for publication. The authors gratefully acknowledge Tzu Ning (Emily) Liu, Chengrui Zou, Gregorio Martinez III, and Zhenjie Liu for their assistance with some of the experiments. The study was conducted at the Perinatology Research Branch, NICHD/NIH/DHHS, in Detroit, Michigan; the Branch has since been renamed as the Pregnancy Research Branch, NICHD/NIH/DHHS.

AUTHOR CONTRIBUTIONS

Conceptualization: J.G. and N.G.-L.; Methodology: J.G., J.M.G., M.A.-H., Y.X., and N.G.-L.; Validation: J.G., J.M.G., M.A.-H., Y.X., and N.G.-L.; Formal analysis: J.G., J.M.G., K.R.T., Y.X., R.R., and N.G.-L.; Investigation: J.G., J.M.G., K.R.T., M.A.-H., Y.X., M.F.-J., D.M., T.K., V.G.-F., and N.G.-L.; Resources: R.R., K.R.T., and N.G.-L.; Data curation: J.G., J.M.G., and Y.X.; Writing – original draft: J.G., D.M., and N.G.-L.; Writing – review & editing: J.G., R.R., J.M.G., K.R.T., M.A.-H., Y.X., M.F.-J., D.M., T.K., V.G.-F., and N.G.-L.; Visualization: J.G., J.M.G., V.G.-F., and N.G.-L.; Supervision: R.R., K.R.T., and N.G.-L.; Project administration: N.G.-L.; Funding acquisition: R.R. and N.G.-L.

DECLARATION OF INTERESTS

The authors declare no competing interests.

INCLUSION AND DIVERSITY

We support inclusive, diverse, and equitable conduct of research.

Received: May 30, 2023
Revised: September 6, 2023
Accepted: October 23, 2023
Published: October 28, 2023

REFERENCES

1. Perin, J., Mulick, A., Yeung, D., Villavicencio, F., Lopez, G., Strong, K.L., Prieto-Merino, D., Cousens, S., Black, R.E., and Liu, L. (2022). Global, regional, and national causes of under-5 mortality in 2000-19: an updated systematic analysis with implications for the Sustainable Development Goals. Lancet. Child Adolesc. Health *6*, 106–115. https://doi.org/10.1016/S2352-4642(21)00311-4.
2. World Health Organization (2022). Child mortality (under 5 years). https://www.who.int/news-room/fact-sheets/detail/levels-and-trends-in-child-under-5-mortality-in-2020#:~:text=Moreover%2C%20the%20youngest%20children%20are,years%20of%20age%20(1).
3. American College of Obstetricians and Gynecologists. (2021). Prediction and Prevention of Spontaneous Preterm Birth: ACOG Practice Bulletin, Number 234. Obstet. Gynecol. *138*, e65–e90. https://doi.org/10.1097/AOG.0000000000004479.
4. March of Dimes (2022). 2022 March of Dimes Report Card. https://www.marchofdimes.org/report-card.
5. Gravett, M.G., and Rubens, C.E.; Global Alliance to Prevent Prematurity and Stillbirth Technical Team (2012). A framework for strategic investments in research to reduce the global burden of preterm birth. Am. J. Obstet. Gynecol. *207*, 368–373. https://doi.org/10.1016/j.ajog.2012.09.008.
6. Harrison, M.S., and Goldenberg, R.L. (2016). Global burden of prematurity. Semin. Fetal Neonatal Med. *21*, 74–79. https://doi.org/10.1016/j.siny.2015.12.007.
7. Waitzman, N.J., Jalali, A., and Grosse, S.D. (2021). Preterm birth lifetime costs in the United States in 2016: An update. Semin. Perinatol. *45*, 151390. https://doi.org/10.1016/j.semperi.2021.151390.
8. Goldenberg, R.L., Culhane, J.F., Iams, J.D., and Romero, R. (2008). Epidemiology and causes of preterm birth. Lancet *371*, 75–84. https://doi.org/10.1016/S0140-6736(08)60074-4.
9. Romero, R., Dey, S.K., and Fisher, S.J. (2014). Preterm labor: one syndrome, many causes. Science *345*, 760–765. https://doi.org/10.1126/science.1251816.
10. Gravett, M.G., Witkin, S.S., Haluska, G.J., Edwards, J.L., Cook, M.J., and Novy, M.J. (1994). An experimental model for intraamniotic infection and preterm labor in rhesus monkeys. Am. J. Obstet. Gynecol. *171*, 1660–1667. https://doi.org/10.1016/0002-9378(94)90418-9.
11. Dudley, D.J., Branch, D.W., Edwin, S.S., and Mitchell, M.D. (1996). Induction of preterm birth in mice by RU486. Biol. Reprod. *55*, 992–995. https://doi.org/10.1095/biolreprod55.5.992.
12. Novy, M.J., Duffy, L., Axthelm, M.K., Sadowsky, D.W., Witkin, S.S., Gravett, M.G., Cassell, G.H., and Waites, K.B. (2009). Ureaplasma parvum or Mycoplasma hominis as sole pathogens cause chorioamnionitis, preterm delivery, and fetal pneumonia in rhesus macaques. Reprod. Sci. *16*, 56–70. https://doi.org/10.1177/1933719108325508.
13. Gomez-Lopez, N., Romero, R., Plazyo, O., Panaitescu, B., Furcron, A.E., Miller, D., Roumayah, T., Flom, E., and Hassan, S.S. (2016). Intra-Amniotic Administration of HMGB1 Induces Spontaneous Preterm Labor and Birth. Am. J. Reprod. Immunol. *75*, 3–7. https://doi.org/10.1111/aji.12443.
14. Boldenow, E., Gendrin, C., Ngo, L., Bierle, C., Vornhagen, J., Coleman, M., Merillat, S., Armistead, B., Whidbey, C., Alishetti, V., et al. (2016). Group B Streptococcus circumvents neutrophils and neutrophil extracellular traps during amniotic cavity invasion and preterm labor. Sci. Immunol. *1*, eaah4576. https://doi.org/10.1126/sciimmunol.aah4576.
15. Garcia-Flores, V., Romero, R., Miller, D., Xu, Y., Done, B., Veerapaneni, C., Leng, Y., Arenas-Hernandez, M., Khan, N., Panaitescu, B., et al. (2018). Inflammation-Induced Adverse Pregnancy and Neonatal Outcomes Can Be Improved by the Immunomodulatory Peptide Exendin-4. Front. Immunol. *9*, 1291. https://doi.org/10.3389/fimmu.2018.01291.
16. Gomez-Lopez, N., Romero, R., Arenas-Hernandez, M., Panaitescu, B., Garcia-Flores, V., Mial, T.N., Sahi, A., and Hassan, S.S. (2018). Intra-amniotic administration of lipopolysaccharide induces spontaneous preterm labor and birth in the absence of a body temperature change. J. Matern. Fetal Neonatal Med. *31*, 439–446. https://doi.org/10.1080/14767058.2017.1287894.
17. Faro, J., Romero, R., Schwenkel, G., Garcia-Flores, V., Arenas-Hernandez, M., Leng, Y., Xu, Y., Miller, D., Hassan, S.S., and Gomez-Lopez, N. (2019). Intra-amniotic inflammation induces preterm birth by activating the NLRP3 inflammasome. Biol. Reprod. *100*, 1290–1305. https://doi.org/10.1093/biolre/ioy261.
18. Gomez-Lopez, N., Romero, R., Garcia-Flores, V., Leng, Y., Miller, D., Hassan, S.S., Hsu, C.D., and Panaitescu, B. (2019). Inhibition of the NLRP3 inflammasome can prevent sterile intra-amniotic inflammation, preterm labor/birth, and adverse neonatal outcomes. Biol. Reprod. *100*, 1306–1318. https://doi.org/10.1093/biolre/ioy264.
19. Motomura, K., Romero, R., Xu, Y., Theis, K.R., Galaz, J., Winters, A.D., Slutsky, R., Garcia-Flores, V., Zou, C., Levenson, D., et al. (2020). Intra-amniotic infection with Ureaplasma parvum causes preterm birth and neonatal mortality that are prevented by treatment with clarithromycin. mBio *11*, e00797-20. https://doi.org/10.1128/mBio.00797-20.
20. Motomura, K., Romero, R., Garcia-Flores, V., Leng, Y., Xu, Y., Galaz, J., Slutsky, R., Levenson, D., and Gomez-Lopez, N. (2020). The alarmin interleukin-1α causes preterm birth through the NLRP3 inflammasome. Mol. Hum. Reprod. *26*, 712–726. https://doi.org/10.1093/molehr/gaaa054.
21. Galaz, J., Romero, R., Arenas-Hernandez, M., Panaitescu, B., Para, R., and Gomez-Lopez, N. (2021). Betamethasone as a potential treatment for preterm birth associated with sterile intra-amniotic inflammation: a murine study. J. Perinat. Med. *49*, 897–906. https://doi.org/10.1515/jpm-2021-0049.
22. Motomura, K., Romero, R., Plazyo, O., Garcia-Flores, V., Gershater, M., Galaz, J., Miller, D., and Gomez-Lopez, N. (2021). The alarmin S100A12 causes sterile inflammation of the human chorioamniotic membranes as well as preterm birth and neonatal mortality in mice. Biol. Reprod. *105*, 1494–1509. https://doi.org/10.1093/biolre/ioab188.
23. Gershater, M., Romero, R., Arenas-Hernandez, M., Galaz, J., Motomura, K., Tao, L., Xu, Y., Miller, D., Pique-Regi, R., Martinez, G., 3rd, et al. (2022). IL-22 Plays a Dual Role in the Amniotic Cavity: Tissue Injury and Host Defense against Microbes in Preterm Labor. J. Immunol. *208*, 1595–1615. https://doi.org/10.4049/jimmunol.2100439.
24. Motomura, K., Romero, R., Galaz, J., Tao, L., Garcia-Flores, V., Xu, Y., Done, B., Arenas-Hernandez, M., Miller, D., Gutierrez-Contreras, P., et al. (2022). Fetal and maternal NLRP3 signaling is required for preterm labor and birth. JCI Insight *7*, e158238. https://doi.org/10.1172/jci.insight.158238.
25. Garcia-Flores, V., Romero, R., Peyvandipour, A., Galaz, J., Pusod, E., Panaitescu, B., Miller, D., Xu, Y., Tao, L., Liu, Z., et al. (2023). A single-cell atlas of murine reproductive tissues during preterm labor. Cell Rep. *42*, 111846. https://doi.org/10.1016/j.celrep.2022.111846.
26. Stranik, J., Kacerovsky, M., Vescicik, P., Faist, T., Jacobsson, B., and Musilova, I. (2022). A rodent model of intra-amniotic inflammation/infection, induced by the administration of inflammatory agent in a gestational sac, associated with preterm delivery: a systematic review. J. Matern. Fetal Neonatal Med. *35*, 1592–1600. https://doi.org/10.1080/14767058.2020.1757063.
27. Romero, R., and Mazor, M. (1988). Infection and preterm labor. Clin. Obstet. Gynecol. *31*, 553–584. https://doi.org/10.1097/00003081-198809000-00006.
28. Romero, R., Gómez, R., Chaiworapongsa, T., Conoscenti, G., Kim, J.C., and Kim, Y.M. (2001). The role of infection in preterm labour and delivery. Paediatr. Perinat. Epidemiol. *15*, 41–56. https://doi.org/10.1046/j.1365-3016.2001.00007.x.
29. Romero, R., Espinoza, J., Gonçalves, L.F., Kusanovic, J.P., Friel, L.A., and Nien, J.K. (2006). Inflammation in preterm and term labour and delivery. Semin. Fetal Neonatal Med. *11*, 317–326. https://doi.org/10.1016/j.siny.2006.05.001.
30. Bastek, J.A., Gómez, L.M., and Elovitz, M.A. (2011). The role of inflammation and infection in preterm birth. Clin. Perinatol. *38*, 385–406. https://doi.org/10.1016/j.clp.2011.06.003.
31. Romero, R., Gomez-Lopez, N., Winters, A.D., Jung, E., Shaman, M., Bieda, J., Panaitescu, B., Pacora, P., Erez, O., Greenberg, J.M., et al. (2019). Evidence that intra-amniotic infections are often the result of an ascending invasion - a molecular microbiological study. J. Perinat. Med. *47*, 915–931. https://doi.org/10.1515/jpm-2019-0297.
32. Matzinger, P. (1998). An innate sense of danger. Semin. Immunol. *10*, 399–415. https://doi.org/10.1006/smim.1998.0143.
33. Rider, P., Voronov, E., Dinarello, C.A., Apte, R.N., and Cohen, I. (2017). Alarmins: Feel the Stress. J. Immunol. *198*, 1395–1402. https://doi.org/10.4049/jimmunol.1601342.
34. Romero, R., Miranda, J., Chaiworapongsa, T., Chaemsaithong, P., Gotsch, F., Dong, Z., Ahmed, A.I., Yoon, B.H., Hassan, S.S., Kim, C.J., et al. (2014). A novel molecular microbiologic technique for the rapid diagnosis of microbial invasion of the amniotic cavity and intra-amniotic infection in preterm labor with intact membranes.

Am. J. Reprod. Immunol. *71*, 330–358. https://doi.org/10.1111/aji.12189.
35. Combs, C.A., Gravett, M., Garite, T.J., Hickok, D.E., Lapidus, J., Porreco, R., Rael, J., Grove, T., Morgan, T.K., Clewell, W., et al. (2014). Amniotic fluid infection, inflammation, and colonization in preterm labor with intact membranes. Am. J. Obstet. Gynecol. *210*, 125.e1. https://doi.org/10.1016/j.ajog.2013.11.032.
36. Romero, R., Miranda, J., Chaiworapongsa, T., Korzeniewski, S.J., Chaemsaithong, P., Gotsch, F., Dong, Z., Ahmed, A.I., Yoon, B.H., Hassan, S.S., et al. (2014). Prevalence and clinical significance of sterile intra-amniotic inflammation in patients with preterm labor and intact membranes. Am. J. Reprod. Immunol. *72*, 458–474. https://doi.org/10.1111/aji.12296.
37. Romero, R., Miranda, J., Chaiworapongsa, T., Chaemsaithong, P., Gotsch, F., Dong, Z., Ahmed, A.I., Yoon, B.H., Hassan, S.S., Kim, C.J., et al. (2015). Sterile intra-amniotic inflammation in asymptomatic patients with a sonographic short cervix: prevalence and clinical significance. J. Matern. Fetal Neonatal Med. *28*, 1343–1359. https://doi.org/10.3109/14767058.2014.954243.
38. Romero, R., Miranda, J., Chaemsaithong, P., Chaiworapongsa, T., Kusanovic, J.P., Dong, Z., Ahmed, A.I., Shaman, M., Lannaman, K., Yoon, B.H., et al. (2015). Sterile and microbial-associated intra-amniotic inflammation in preterm prelabor rupture of membranes. J. Matern. Fetal Neonatal Med. *28*, 1394–1409. https://doi.org/10.3109/14767058.2014.958463.
39. Burnham, P., Gomez-Lopez, N., Heyang, M., Cheng, A.P., Lenz, J.S., Dadhania, D.M., Lee, J.R., Suthanthiran, M., Romero, R., and De Vlaminck, I. (2020). Separating the signal from the noise in metagenomic cell-free DNA sequencing. Microbiome *8*, 18. https://doi.org/10.1186/s40168-020-0793-4.
40. Arenas-Hernandez, M., Romero, R., Xu, Y., Panaitescu, B., Garcia-Flores, V., Miller, D., Ahn, H., Done, B., Hassan, S.S., Hsu, C.D., et al. (2019). Effector and Activated T Cells Induce Preterm Labor and Birth That Is Prevented by Treatment with Progesterone. J. Immunol. *202*, 2585–2608. https://doi.org/10.4049/jimmunol.1801350.
41. Elovitz, M.A., Gajer, P., Riis, V., Brown, A.G., Humphrys, M.S., Holm, J.B., and Ravel, J. (2019). Cervicovaginal microbiota and local immune response modulate the risk of spontaneous preterm delivery. Nat. Commun. *10*, 1305. https://doi.org/10.1038/s41467-019-09285-9.
42. Fettweis, J.M., Serrano, M.G., Brooks, J.P., Edwards, D.J., Girerd, P.H., Parikh, H.I., Huang, B., Arodz, T.J., Edupuganti, L., Glascock, A.L., et al. (2019). The vaginal microbiome and preterm birth. Nat. Med. *25*, 1012–1021. https://doi.org/10.1038/s41591-019-0450-2.
43. Pruski, P., Correia, G.D.S., Lewis, H.V., Capuccini, K., Inglese, P., Chan, D., Brown, R.G., Kindinger, L., Lee, Y.S., Smith, A., et al. (2021). Direct on-swab metabolic profiling of vaginal microbiome host interactions during pregnancy and preterm birth. Nat. Commun. *12*, 5967. https://doi.org/10.1038/s41467-021-26215-w.
44. Flaviani, F., Hezelgrave, N.L., Kanno, T., Prosdocimi, E.M., Chin-Smith, E., Ridout, A.E., von Maydell, D.K., Mistry, V., Wade, W.G., Shennan, A.H., et al. (2021). Cervicovaginal microbiota and metabolome predict preterm birth risk in an ethnically diverse cohort. JCI Insight *6*, e149257. https://doi.org/10.1172/jci.insight.149257.
45. Payne, M.S., Newnham, J.P., Doherty, D.A., Furfaro, L.L., Pendal, N.L., Loh, D.E., and Keelan, J.A. (2021). A specific bacterial DNA signature in the vagina of Australian women in midpregnancy predicts high risk of spontaneous preterm birth (the Predict1000 study). Am. J. Obstet. Gynecol. *224*, 206.e1. https://doi.org/10.1016/j.ajog.2020.08.034.
46. Chan, D., Bennett, P.R., Lee, Y.S., Kundu, S., Teoh, T.G., Adan, M., Ahmed, S., Brown, R.G., David, A.L., Lewis, H.V., et al. (2022). Microbial-driven preterm labour involves crosstalk between the innate and adaptive immune response. Nat. Commun. *13*, 975. https://doi.org/10.1038/s41467-022-28620-1.
47. Lamont, R.F., Richardson, L.S., Boniface, J.J., Cobo, T., Exner, M.M., Christensen, I.B., Forslund, S.K., Gaba, A., Helmer, H., Jørgensen, J.S., et al. (2020). Commentary on a combined approach to the problem of developing biomarkers for the prediction of spontaneous preterm labor that leads to preterm birth. Placenta *98*, 13–23. https://doi.org/10.1016/j.placenta.2020.05.007.
48. Romero, R., Tarca, A., Gomez-Lopez, N., Winters, A., Panzer, J., Lin, H., Gudicha, D., Galaz, J., Farias-Jofre, M., Kracht, D., et al. (2022). The Vaginal Microbiota in Early Pregnancy Identifies a Subset of Women at Risk for Early Preterm Prelabor Rupture of Membranes and Preterm Birth. Preprint at Research Square. https://doi.org/10.21203/rs.3.rs-2359402/v1.
49. Shaffer, Z., Romero, R., Tarca, A., Galaz, J., Arenas-Hernandez, M., Gudicha, D., Chaiworapongsa, T., Jung, E., Suksai, M., Gotsch, F., et al. (2022). The Vaginal Immunoproteome for the Prediction of Spontaneous Preterm Birth. Preprint at bioRxiv. https://doi.org/10.2139/ssrn.4259790.
50. Romero, R., Mazor, M., Munoz, H., Gomez, R., Galasso, M., and Sherer, D.M. (1994). The preterm labor syndrome. Ann. N. Y. Acad. Sci. *734*, 414–429. https://doi.org/10.1111/j.1749-6632.1994.tb21771.x.
51. Norwitz, E.R., Robinson, J.N., and Challis, J.R. (1999). The control of labor. N. Engl. J. Med. *341*, 660–666. https://doi.org/10.1056/NEJM199908263410906.
52. Romero, R., Espinoza, J., Kusanovic, J.P., Gotsch, F., Hassan, S., Erez, O., Chaiworapongsa, T., and Mazor, M. (2006). The preterm parturition syndrome. BJOG *113*, 17–42. https://doi.org/10.1111/j.1471-0528.2006.01120.x.
53. Smith, R. (2007). Parturition. N. Engl. J. Med. *356*, 271–283. https://doi.org/10.1056/NEJMra061360.
54. Cunningham, F.G., Leveno, K.J., Bloom, S.L., Dashe, J.S., Hoffman, B.L., Casey, B.M., and Spong, C.Y., eds. (2018). Normal Labor. In Williams Obstetrics, 25e (McGraw-Hill Education).
55. Pierce, S.L., Kutschke, W., Cabeza, R., and England, S.K. (2010). In vivo measurement of intrauterine pressure by telemetry: a new approach for studying parturition in mouse models. Physiol. Genomics *42*, 310–316. https://doi.org/10.1152/physiolgenomics.00058.2010.
56. Robuck, M.F., O'Brien, C.M., Knapp, K.M., Shay, S.D., West, J.D., Newton, J.M., Slaughter, J.C., Paria, B.C., Reese, J., and Herington, J.L. (2018). Monitoring uterine contractility in mice using a transcervical intrauterine pressure catheter. Reproduction *155*, 447–456. https://doi.org/10.1530/rep-17-0647.
57. Yoshida, K., Jayyosi, C., Lee, N., Mahendroo, M., and Myers, K.M. (2019). Mechanics of cervical remodelling: insights from rodent models of pregnancy. Interface Focus *9*, 20190026. https://doi.org/10.1098/rsfs.2019.0026.
58. Rhoades, J.S., and Cahill, A.G. (2017). Defining and Managing Normal and Abnormal First Stage of Labor. Obstet. Gynecol. Clin. North Am. *44*, 535–545. https://doi.org/10.1016/j.ogc.2017.07.001.
59. Caughey, A.B. (2020). Is Zhang the new Friedman: How should we evaluate the first stage of labor? Semin. Perinatol. *44*, 151215. https://doi.org/10.1016/j.semperi.2019.151215.
60. Romero, R., Grivel, J.C., Tarca, A.L., Chaemsaithong, P., Xu, Z., Fitzgerald, W., Hassan, S.S., Chaiworapongsa, T., and Margolis, L. (2015). Evidence of perturbations of the cytokine network in preterm labor. Am. J. Obstet. Gynecol. *213*, 836.e1–836.e18. https://doi.org/10.1016/j.ajog.2015.07.037.
61. Bhatti, G., Romero, R., Rice, G.E., Fitzgerald, W., Pacora, P., Gomez-Lopez, N., Kavdia, M., Tarca, A.L., and Margolis, L. (2020). Compartmentalized profiling of amniotic fluid cytokines in women with preterm labor. PLoS One *15*, e0227881. https://doi.org/10.1371/journal.pone.0227881.
62. Romero, R., Brody, D.T., Oyarzun, E., Mazor, M., Wu, Y.K., Hobbins, J.C., and Durum, S.K. (1989). Infection and labor. III. Interleukin-1: a signal for the onset of parturition. Am. J. Obstet. Gynecol. *160*, 1117–1123. https://doi.org/10.1016/0002-9378(89)90172-5.
63. Fortunato, S.J., and Menon, R. (2001). Distinct molecular events suggest different pathways for preterm labor and premature rupture of membranes. Am. J. Obstet. Gynecol. *184*, 1399–1405. , discussion 1405-6. https://doi.org/10.1067/mob.2001.115122.
64. Romero, R., Chaiworapongsa, T., Alpay Savasan, Z., Xu, Y., Hussein, Y., Dong, Z., Kusanovic, J.P., Kim, C.J., and Hassan, S.S. (2011). Damage-associated molecular patterns (DAMPs) in preterm labor with intact membranes and preterm PROM: a study of the alarmin HMGB1. J. Matern. Fetal Neonatal Med. *24*, 1444–1455. https://doi.org/10.3109/14767058.2011.591460.
65. Romero, R., Ghidini, A., Mazor, M., and Behnke, E. (1991). Microbial invasion of the amniotic cavity in premature rupture of membranes. Clin. Obstet. Gynecol. *34*, 769–778. https://doi.org/10.1097/00003081-199112000-00013.
66. DiGiulio, D.B., Romero, R., Kusanovic, J.P., Gómez, R., Kim, C.J., Seok, K.S., Gotsch, F., Mazaki-Tovi, S., Vaisbuch, E., Sanders, K., et al. (2010). Prevalence and diversity of microbes in the amniotic fluid, the fetal inflammatory response, and pregnancy outcome in women with preterm pre-labor rupture of membranes. Am. J. Reprod. Immunol. *64*, 38–57. https://doi.org/10.1111/j.1600-0897.2010.00830.x.
67. Sierra, L.J., Brown, A.G., Barilá, G.O., Anton, L., Barnum, C.E., Shetye, S.S., Soslowsky, L.J., and Elovitz, M.A. (2018). Colonization of the cervicovaginal space with Gardnerella vaginalis leads to local inflammation and

cervical remodeling in pregnant mice. PLoS One *13*, e0191524. https://doi.org/10.1371/journal.pone.0191524.

68. Florova, V., Romero, R., Tarca, A.L., Galaz, J., Motomura, K., Ahmad, M.M., Hsu, C.D., Hsu, R., Tong, A., Ravel, J., et al. (2021). Vaginal host immune-microbiome interactions in a cohort of primarily African-American women who ultimately underwent spontaneous preterm birth or delivered at term. Cytokine *137*, 155316. https://doi.org/10.1016/j.cyto.2020.155316.
69. Anton, L., Ferguson, B., Friedman, E.S., Gerson, K.D., Brown, A.G., and Elovitz, M.A. (2022). Gardnerella vaginalis alters cervicovaginal epithelial cell function through microbe-specific immune responses. Microbiome *10*, 119. https://doi.org/10.1186/s40168-022-01317-9.
70. Gonzalez, J.M., Xu, H., Chai, J., Ofori, E., and Elovitz, M.A. (2009). Preterm and term cervical ripening in CD1 Mice (Mus musculus): similar or divergent molecular mechanisms? Biol. Reprod. *81*, 1226–1232. https://doi.org/10.1095/biolreprod.108.075309.
71. Akgul, Y., Word, R.A., Ensign, L.M., Yamaguchi, Y., Lydon, J., Hanes, J., and Mahendroo, M. (2014). Hyaluronan in cervical epithelia protects against infection-mediated preterm birth. J. Clin. Invest. *124*, 5481–5489. https://doi.org/10.1172/JCI78765.
72. Willcockson, A.R., Nandu, T., Liu, C.L., Nallasamy, S., Kraus, W.L., and Mahendroo, M. (2018). Transcriptome signature identifies distinct cervical pathways induced in lipopolysaccharide-mediated preterm birth. Biol. Reprod. *98*, 408–421. https://doi.org/10.1093/biolre/iox180.
73. Vink, J.Y., Qin, S., Brock, C.O., Zork, N.M., Feltovich, H.M., Chen, X., Urie, P., Myers, K.M., Hall, T.J., Wapner, R., et al. (2016). A new paradigm for the role of smooth muscle cells in the human cervix. Am. J. Obstet. Gynecol. *215*, 478.e1–478.e11. https://doi.org/10.1016/j.ajog.2016.04.053.
74. Gonzalez, J.M., Franzke, C.W., Yang, F., Romero, R., and Girardi, G. (2011). Complement activation triggers metalloproteinases release inducing cervical remodeling and preterm birth in mice. Am. J. Pathol. *179*, 838–849. https://doi.org/10.1016/j.ajpath.2011.04.024.
75. Jeong, H.C., Kim, H.Y., Kim, H.Y., Wang, E.J., Ahn, K.H., Oh, M.J., Choi, B.M., and Kim, H.J. (2021). Changes in gene expression of cervical collagens, metalloproteinases, and tissue inhibitors of metalloproteinases after partial cervical excision-induced preterm labor in mice. PLoS One *16*, e0250108. https://doi.org/10.1371/journal.pone.0250108.
76. Tantengco, O.A.G., Kechichian, T., Vincent, K.L., Pyles, R.B., Medina, P.M.B., and Menon, R. (2021). Inflammatory response elicited by Ureaplasma parvum colonization in human cervical epithelial, stromal, and immune cells. Reproduction *163*, 1–10. https://doi.org/10.1530/REP-21-0308.
77. Leppert, P.C., Kokenyesi, R., Klemenich, C.A., and Fisher, J. (2000). Further evidence of a decorin-collagen interaction in the disruption of cervical collagen fibers during rat gestation. Am. J. Obstet. Gynecol. *182*, 805–811. , discussion 811-2. https://doi.org/10.1016/s0002-9378(00)70329-2.
78. Timmons, B.C., Mitchell, S.M., Gilpin, C., and Mahendroo, M.S. (2007). Dynamic changes in the cervical epithelial tight junction complex and differentiation occur during cervical ripening and parturition. Endocrinology *148*, 1278–1287. https://doi.org/10.1210/en.2006-0851.
79. Read, C.P., Word, R.A., Ruscheinsky, M.A., Timmons, B.C., and Mahendroo, M.S. (2007). Cervical remodeling during pregnancy and parturition: molecular characterization of the softening phase in mice. Reproduction *134*, 327–340. https://doi.org/10.1530/REP-07-0032.
80. Colon-Caraballo, M., Lee, N., Nallasamy, S., Myers, K., Hudson, D., Iozzo, R.V., and Mahendroo, M. (2022). Novel regulatory roles of small leucine-rich proteoglycans in remodeling of the uterine cervix in pregnancy. Matrix Biol. *105*, 53–71. https://doi.org/10.1016/j.matbio.2021.11.004.
81. Pruski, P., Lewis, H.V., Lee, Y.S., Marchesi, J.R., Bennett, P.R., Takats, Z., and MacIntyre, D.A. (2018). Assessment of microbiota:host interactions at the vaginal mucosa interface. Methods *149*, 74–84. https://doi.org/10.1016/j.ymeth.2018.04.022.
82. Grewal, K., MacIntyre, D.A., and Bennett, P.R. (2021). The reproductive tract microbiota in pregnancy. Biosci. Rep. *41*. https://doi.org/10.1042/BSR20203908.
83. Dong, M., Dong, Y., Bai, J., Li, H., Ma, X., Li, B., Wang, C., Li, H., Qi, W., Wang, Y., et al. (2023). Interactions between microbiota and cervical epithelial, immune, and mucus barrier. Front. Cell. Infect. Microbiol. *13*, 1124591. https://doi.org/10.3389/fcimb.2023.1124591.
84. Seong, H.S., Lee, S.E., Kang, J.H., Romero, R., and Yoon, B.H. (2008). The frequency of microbial invasion of the amniotic cavity and histologic chorioamnionitis in women at term with intact membranes in the presence or absence of labor. Am. J. Obstet. Gynecol. *199*, 375.e1–375.e5. https://doi.org/10.1016/j.ajog.2008.06.040.
85. Lee, S.M., Lee, K.A., Kim, S.M., Park, C.W., and Yoon, B.H. (2011). The risk of intra-amniotic infection, inflammation and histologic chorioamnionitis in term pregnant women with intact membranes and labor. Placenta *32*, 516–521. https://doi.org/10.1016/j.placenta.2011.03.012.
86. Liggins, G.C. (1983). Initiation of spontaneous labor. Clin. Obstet. Gynecol. *26*, 47–55. https://doi.org/10.1097/00003081-198303000-00009.
87. Norwitz, E.R., Bonney, E.A., Snegovskikh, V.V., Williams, M.A., Phillippe, M., Park, J.S., and Abrahams, V.M. (2015). Molecular Regulation of Parturition: The Role of the Decidual Clock. Cold Spring Harb. Perspect. Med. *5*, a023143. https://doi.org/10.1101/cshperspect.a023143.
88. Stelzer, I.A., Ghaemi, M.S., Han, X., Ando, K., Hédou, J.J., Feyaerts, D., Peterson, L.S., Rumer, K.K., Tsai, E.S., Ganio, E.A., et al. (2021). Integrated trajectories of the maternal metabolome, proteome, and immunome predict labor onset. Sci. Transl. Med. *13*, eabd9898. https://doi.org/10.1126/scitranslmed.abd9898.
89. Smith, S.B., and Ravel, J. (2017). The vaginal microbiota, host defence and reproductive physiology. J. Physiol. *595*, 451–463. https://doi.org/10.1113/JP271694.
90. Anahtar, M.N., Gootenberg, D.B., Mitchell, C.M., and Kwon, D.S. (2018). Cervicovaginal Microbiota and Reproductive Health: The Virtue of Simplicity. Cell Host Microbe *23*, 159–168. https://doi.org/10.1016/j.chom.2018.01.013.
91. Monin, L., Whettlock, E.M., and Male, V. (2020). Immune responses in the human female reproductive tract. Immunology *160*, 106–115. https://doi.org/10.1111/imm.13136.
92. France, M., Alizadeh, M., Brown, S., Ma, B., and Ravel, J. (2022). Towards a deeper understanding of the vaginal microbiota. Nat. Microbiol. *7*, 367–378. https://doi.org/10.1038/s41564-022-01083-2.
93. Kumar, M., Murugesan, S., Singh, P., Saadaoui, M., Elhag, D.A., Terranegra, A., Kabeer, B.S.A., Marr, A.K., Kino, T., Brummaier, T., et al. (2021). Vaginal Microbiota and Cytokine Levels Predict Preterm Delivery in Asian Women. Front. Cell. Infect. Microbiol. *11*, 639665. https://doi.org/10.3389/fcimb.2021.639665.
94. Pinto, S., Malheiro, M.F., Vaz, A., Rodrigues, T., Montenegro, N., and Guimarães, H. (2019). Neonatal outcome in preterm deliveries before 34-week gestation - the influence of the mechanism of labor onset. J. Matern. Fetal Neonatal Med. *32*, 3655–3661. https://doi.org/10.1080/14767058.2018.1481038.
95. Goya, M., Bernabeu, A., García, N., Plata, J., Gonzalez, F., Merced, C., Llurba, E., Suy, A., Casellas, M., Carreras, E., and Cabero, L. (2013). Premature rupture of membranes before 34 weeks managed expectantly: maternal and perinatal outcomes in singletons. J. Matern. Fetal Neonatal Med. *26*, 290–293. https://doi.org/10.3109/14767058.2012.733779.
96. Cobo, T., Vergara, A., Collado, M.C., Casals-Pascual, C., Herreros, E., Bosch, J., Sánchez-García, A.B., López-Parellada, R., Ponce, J., and Gratacós, E. (2019). Characterization of vaginal microbiota in women with preterm labor with intra-amniotic inflammation. Sci. Rep. *9*, 18963. https://doi.org/10.1038/s41598-019-55611-y.
97. Thaiss, C.A., Levy, M., Korem, T., Dohnalová, L., Shapiro, H., Jaitin, D.A., David, E., Winter, D.R., Gury-BenAri, M., Tatirovsky, E., et al. (2016). Microbiota Diurnal Rhythmicity Programs Host Transcriptome Oscillations. Cell *167*, 1495–1510.e12. https://doi.org/10.1016/j.cell.2016.11.003.
98. Heddes, M., Altaha, B., Niu, Y., Reitmeier, S., Kleigrewe, K., Haller, D., and Kiessling, S. (2022). The intestinal clock drives the microbiome to maintain gastrointestinal homeostasis. Nat. Commun. *13*, 6068. https://doi.org/10.1038/s41467-022-33609-x.
99. Motomura, K., Romero, R., Galaz, J., Tarca, A.L., Done, B., Xu, Y., Leng, Y., Garcia-Flores, V., Arenas-Hernandez, M., Theis, K.R., et al. (2021). RNA Sequencing Reveals Distinct Immune Responses in the Chorioamniotic Membranes of Women with Preterm Labor and Microbial or Sterile Intra-amniotic Inflammation. Infect. Immun. *89*, e00819-20. https://doi.org/10.1128/IAI.00819-20.
100. Gravett, M.G., Adams, K.M., Sadowsky, D.W., Grosvenor, A.R., Witkin, S.S., Axthelm, M.K., and Novy, M.J. (2007). Immunomodulators plus antibiotics delay preterm delivery after experimental intraamniotic infection in a nonhuman primate model. Am. J. Obstet. Gynecol. *197*, 518.e1–518.e8. https://doi.org/10.1016/j.ajog.2007.03.064.

101. Schwenkel, G., Romero, R., Slutsky, R., Motomura, K., Hsu, C.D., and Gomez-Lopez, N. (2021). HSP70: an alarmin that does not induce high rates of preterm birth but does cause adverse neonatal outcomes. J. Matern. Fetal Neonatal Med. *34*, 4110–4118. https://doi.org/10.1080/14767058.2019.1706470.

102. Galaz, J., Romero, R., Arenas-Hernandez, M., Farias-Jofre, M., Motomura, K., Liu, Z., Kawahara, N., Demery-Poulos, C., Liu, T.N., Padron, J., et al. (2022). Clarithromycin prevents preterm birth and neonatal mortality by dampening alarmin-induced maternal-fetal inflammation in mice. BMC Pregnancy Childbirth *22*, 503. https://doi.org/10.1186/s12884-022-04764-2.

103. Galaz, J., Motomura, K., Romero, R., Liu, Z., Garcia-Flores, V., Tao, L., Xu, Y., Done, B., Arenas-Hernandez, M., Kanninen, T., et al. (2023). A key role for NLRP3 signaling in preterm labor and birth driven by the alarmin S100B. Transl. Res. *259*, 46–61. https://doi.org/10.1016/j.trsl.2023.04.004.

104. Burd, I., Bentz, A.I., Chai, J., Gonzalez, J., Monnerie, H., Le Roux, P.D., Cohen, A.S., Yudkoff, M., and Elovitz, M.A. (2010). Inflammation-induced preterm birth alters neuronal morphology in the mouse fetal brain. J. Neurosci. Res. *88*, 1872–1881. https://doi.org/10.1002/jnr.22368.

105. Hassan, S.S., Romero, R., Tarca, A.L., Nhan-Chang, C.L., Vaisbuch, E., Erez, O., Mittal, P., Kusanovic, J.P., Mazaki-Tovi, S., Yeo, L., et al. (2009). The transcriptome of cervical ripening in human pregnancy before the onset of labor at term: identification of novel molecular functions involved in this process. J. Matern. Fetal Neonatal Med. *22*, 1183–1193. https://doi.org/10.3109/14767050903353216.

106. Hassan, S.S., Romero, R., Tarca, A.L., Nhan-Chang, C.L., Mittal, P., Vaisbuch, E., Gonzalez, J.M., Chaiworapongsa, T., Ali-Fehmi, R., Dong, Z., et al. (2010). The molecular basis for sonographic cervical shortening at term: identification of differentially expressed genes and the epithelial-mesenchymal transition as a function of cervical length. Am. J. Obstet. Gynecol. *203*, 472.e1–472.e14. https://doi.org/10.1016/j.ajog.2010.06.076.

107. Hassan, S.S., Romero, R., Haddad, R., Hendler, I., Khalek, N., Tromp, G., Diamond, M.P., Sorokin, Y., and Malone, J., Jr. (2006). The transcriptome of the uterine cervix before and after spontaneous term parturition. Am. J. Obstet. Gynecol. *195*, 778–786. https://doi.org/10.1016/j.ajog.2006.06.021.

108. Junqueira, L.C., Zugaib, M., Montes, G.S., Toledo, O.M., Krisztán, R.M., and Shigihara, K.M. (1980). Morphologic and histochemical evidence for the occurrence of collagenolysis and for the role of neutrophilic polymorphonuclear leukocytes during cervical dilation. Am. J. Obstet. Gynecol. *138*, 273–281. https://doi.org/10.1016/0002-9378(80)90248-3.

109. Liggins, C.G. (1981). Cervical ripening as an inflammatory reaction. In Cervix in Pregnancy and Labour, D.A. Elwood and A.B.M. Andersson, eds. (Churchill Livingstone), pp. 1–9.

110. Bokström, H., Brännström, M., Alexandersson, M., and Norström, A. (1997). Leukocyte subpopulations in the human uterine cervical stroma at early and term pregnancy. Hum. Reprod. *12*, 586–590. https://doi.org/10.1093/humrep/12.3.586.

111. Osman, I., Young, A., Ledingham, M.A., Thomson, A.J., Jordan, F., Greer, I.A., and Norman, J.E. (2003). Leukocyte density and pro-inflammatory cytokine expression in human fetal membranes, decidua, cervix and myometrium before and during labour at term. Mol. Hum. Reprod. *9*, 41–45. https://doi.org/10.1093/molehr/gag001.

112. Sakamoto, Y., Moran, P., Bulmer, J.N., Searle, R.F., and Robson, S.C. (2005). Macrophages and not granulocytes are involved in cervical ripening. J. Reprod. Immunol. *66*, 161–173. https://doi.org/10.1016/j.jri.2005.04.005.

113. Yellon, S.M., Ebner, C.A., and Sugimoto, Y. (2008). Parturition and recruitment of macrophages in cervix of mice lacking the prostaglandin F receptor. Biol. Reprod. *78*, 438–444. https://doi.org/10.1095/biolreprod.107.063404.

114. Timmons, B.C., Fairhurst, A.M., and Mahendroo, M.S. (2009). Temporal changes in myeloid cells in the cervix during pregnancy and parturition. J. Immunol. *182*, 2700–2707. https://doi.org/10.4049/jimmunol.0803138.

115. Gonzalez, J.M., Dong, Z., Romero, R., and Girardi, G. (2011). Cervical remodeling/ripening at term and preterm delivery: the same mechanism initiated by different mediators and different effector cells. PLoS One *6*, e26877. https://doi.org/10.1371/journal.pone.0026877.

116. Myers, D.A. (2012). The recruitment and activation of leukocytes into the immune cervix: further support that cervical remodeling involves an immune and inflammatory mechanism. Biol. Reprod. *87*, 107. https://doi.org/10.1095/biolreprod.112.105049.

117. Payne, K.J., Clyde, L.A., Weldon, A.J., Milford, T.A., and Yellon, S.M. (2012). Residency and activation of myeloid cells during remodeling of the prepartum murine cervix. Biol. Reprod. *87*, 106. https://doi.org/10.1095/biolreprod.112.101840.

118. Romero, R., Mazor, M., Wu, Y.K., Sirtori, M., Oyarzun, E., Mitchell, M.D., and Hobbins, J.C. (1988). Infection in the pathogenesis of preterm labor. Semin. Perinatol. *12*, 262–279.

119. Goldenberg, R.L., Hauth, J.C., and Andrews, W.W. (2000). Intrauterine infection and preterm delivery. N. Engl. J. Med. *342*, 1500–1507. https://doi.org/10.1056/NEJM200005183422007.

120. Reznikov, L.L., Fantuzzi, G., Selzman, C.H., Shames, B.D., Barton, H.A., Bell, H., McGregor, J.A., and Dinarello, C.A. (1999). Utilization of endoscopic inoculation in a mouse model of intrauterine infection-induced preterm birth: role of interleukin 1beta. Biol. Reprod. *60*, 1231–1238. https://doi.org/10.1095/biolreprod60.5.1231.

121. Fidel, P., Ghezzi, F., Romero, R., Chaiworapongsa, T., Espinoza, J., Cutright, J., Wolf, N., and Gomez, R. (2003). The effect of antibiotic therapy on intrauterine infection-induced preterm parturition in rabbits. J. Matern. Fetal Neonatal Med. *14*, 57–64. https://doi.org/10.1080/jmf.14.1.57.64.

122. Pavlidis, I., Spiller, O.B., Sammut Demarco, G., MacPherson, H., Howie, S.E.M., Norman, J.E., and Stock, S.J. (2020). Cervical epithelial damage promotes Ureaplasma parvum ascending infection, intrauterine inflammation and preterm birth induction in mice. Nat. Commun. *11*, 199. https://doi.org/10.1038/s41467-019-14089-y.

123. Suff, N., Karda, R., Diaz, J.A., Ng, J., Baruteau, J., Perocheau, D., Taylor, P.W., Alber, D., Buckley, S.M.K., Bajaj-Elliott, M., et al. (2020). Cervical Gene Delivery of the Antimicrobial Peptide, Human beta-Defensin (HBD)-3, in a Mouse Model of Ascending Infection-Related Preterm Birth. Front. Immunol. *11*, 106. https://doi.org/10.3389/fimmu.2020.00106.

124. Spencer, N.R., Radnaa, E., Baljinnyam, T., Kechichian, T., Tantengco, O.A.G., Bonney, E., Kammala, A.K., Sheller-Miller, S., and Menon, R. (2021). Development of a mouse model of ascending infection and preterm birth. PLoS One *16*, e0260370. https://doi.org/10.1371/journal.pone.0260370.

125. Anton, L., Sierra, L.J., DeVine, A., Barila, G., Heiser, L., Brown, A.G., and Elovitz, M.A. (2018). Common Cervicovaginal Microbial Supernatants Alter Cervical Epithelial Function: Mechanisms by Which Lactobacillus crispatus Contributes to Cervical Health. Front. Microbiol. *9*, 2181. https://doi.org/10.3389/fmicb.2018.02181.

126. Gilbert, N.M., Foster, L.R., Cao, B., Yin, Y., Mysorekar, I.U., and Lewis, A.L. (2021). Gardnerella vaginalis promotes group B Streptococcus vaginal colonization, enabling ascending uteroplacental infection in pregnant mice. Am. J. Obstet. Gynecol. *224*, 530.e1–530.e17. https://doi.org/10.1016/j.ajog.2020.11.032.

127. Tantengco, O.A.G., Richardson, L.S., Radnaa, E., Kammala, A.K., Kim, S., Medina, P.M.B., Han, A., and Menon, R. (2022). Modeling ascending Ureaplasma parvum infection through the female reproductive tract using vagina-cervix-decidua-organ-on-a-chip and feto-maternal interface-organ-on-a-chip. FASEB J *36*, e22551. https://doi.org/10.1096/fj.202200872R.

128. Holt, R., Timmons, B.C., Akgul, Y., Akins, M.L., and Mahendroo, M. (2011). The molecular mechanisms of cervical ripening differ between term and preterm birth. Endocrinology *152*, 1036–1046. https://doi.org/10.1210/en.2010-1105.

129. Nallasamy, S., Akins, M., Tetreault, B., Luby-Phelps, K., and Mahendroo, M. (2018). Distinct reorganization of collagen architecture in lipopolysaccharide-mediated premature cervical remodeling. Biol. Reprod. *98*, 63–74. https://doi.org/10.1093/biolre/iox155.

130. Zierden, H.C., Ortiz Ortiz, J.I., Dimitrion, P., Laney, V., Bensouda, S., Anders, N.M., Scardina, M., Hoang, T., Ronnett, B.M., Hanes, J., et al. (2020). Characterization of an Adapted Murine Model of Intrauterine Inflammation-Induced Preterm Birth. Am. J. Pathol. *190*, 295–305. https://doi.org/10.1016/j.ajpath.2019.10.013.

131. Egli, G.E., and Newton, M. (1961). The transport of carbon particles in the human female reproductive tract. Fertil. Steril. *12*, 151–155. https://doi.org/10.1016/s0015-0282(16)34084-5.

132. Friedman, E. (1954). The graphic analysis of labor. Am. J. Obstet. Gynecol. *68*, 1568–1575. https://doi.org/10.1016/0002-9378(54)90311-7.

133. Zhang, J., Landy, H.J., Ware Branch, D., Burkman, R., Haberman, S., Gregory, K.D., Hatjis, C.G., Ramirez, M.M., Bailit, J.L., Gonzalez-Quintero, V.H., et al. (2010). Contemporary patterns of spontaneous

labor with normal neonatal outcomes. Obstet. Gynecol. *116*, 1281–1287. https://doi.org/10.1097/AOG.0b013e3181fdef6e.

134. Cohen, W.R., and Friedman, E.A. (2023). The latent phase of labor. Am. J. Obstet. Gynecol. *228*. S1017–s1024. https://doi.org/10.1016/j.ajog.2022.04.029.
135. Friedman, E.A., and Cohen, W.R. (2023). The active phase of labor. Am. J. Obstet. Gynecol. *228*. S1037–s1049. https://doi.org/10.1016/j.ajog.2021.12.269.
136. Galaz, J., Romero, R., Arenas-Hernandez, M., Panaitescu, B., Garcia-Flores, V., and Gomez-Lopez, N. (2020). A Protocol for Evaluating Vital Signs and Maternal-Fetal Parameters Using High-Resolution Ultrasound in Pregnant Mice. STAR Protoc. *1*, 100134. https://doi.org/10.1016/j.xpro.2020.100134.
137. Gomez-Lopez, N., Arenas-Hernandez, M., Romero, R., Miller, D., Garcia-Flores, V., Leng, Y., Xu, Y., Galaz, J., Hassan, S.S., Hsu, C.D., et al. (2020). Regulatory T Cells Play a Role in a Subset of Idiopathic Preterm Labor/Birth and Adverse Neonatal Outcomes. Cell Rep. *32*, 107874. https://doi.org/10.1016/j.celrep.2020.107874.
138. Gomez-Lopez, N., Romero, R., Schwenkel, G., Garcia-Flores, V., Panaitescu, B., Varrey, A., Ayoub, F., Hassan, S.S., and Phillippe, M. (2020). Cell-Free Fetal DNA Increases Prior to Labor at Term and in a Subset of Preterm Births. Reprod. Sci. *27*, 218–232. https://doi.org/10.1007/s43032-019-00023-6.
139. Gomez-Lopez, N., Garcia-Flores, V., Chin, P.Y., Groome, H.M., Bijland, M.T., Diener, K.R., Romero, R., and Robertson, S.A. (2021). Macrophages exert homeostatic actions in pregnancy to protect against preterm birth and fetal inflammatory injury. JCI Insight *6*, e146089. https://doi.org/10.1172/jci.insight.146089.
140. Theis, K.R., Romero, R., Greenberg, J.M., Winters, A.D., Garcia-Flores, V., Motomura, K., Ahmad, M.M., Galaz, J., Arenas-Hernandez, M., and Gomez-Lopez, N. (2020). No Consistent Evidence for Microbiota in Murine Placental and Fetal Tissues. mSphere *5*, e00933. https://doi.org/10.1128/mSphere.00933-19.
141. Theis, K.R., Romero, R., Winters, A.D., Jobe, A.H., and Gomez-Lopez, N. (2020). Lack of Evidence for Microbiota in the Placental and Fetal Tissues of Rhesus Macaques. mSphere *5*, e00210-20. https://doi.org/10.1128/mSphere.00210-20.
142. Greenberg, J.M., Romero, R., Winters, A.D., Galaz, J., Garcia-Flores, V., Arenas-Hernandez, M., Panzer, J., Shaffer, Z., Kracht, D.J., Gomez-Lopez, N., and Theis, K.R. (2022). Microbiota of the Pregnant Mouse: Characterization of the Bacterial Communities in the Oral Cavity, Lung, Intestine, and Vagina through Culture and DNA Sequencing. Microbiol. Spectr. *10*, e0128622. https://doi.org/10.1128/spectrum.01286-22.
143. Kozich, J.J., Westcott, S.L., Baxter, N.T., Highlander, S.K., and Schloss, P.D. (2013). Development of a dual-index sequencing strategy and curation pipeline for analyzing amplicon sequence data on the MiSeq Illumina sequencing platform. Appl. Environ. Microbiol. *79*, 5112–5120. https://doi.org/10.1128/AEM.01043-13.
144. Callahan, B.J., McMurdie, P.J., Rosen, M.J., Han, A.W., Johnson, A.J.A., and Holmes, S.P. (2016). DADA2: High-resolution sample inference from Illumina amplicon data. Nat. Methods *13*, 581–583. https://doi.org/10.1038/nmeth.3869.
145. Winters, A.D., Romero, R., Greenberg, J.M., Galaz, J., Shaffer, Z.D., Garcia-Flores, V., Kracht, D.J., Gomez-Lopez, N., and Theis, K.R. (2022). Does the Amniotic Fluid of Mice Contain a Viable Microbiota? Front. Immunol. *13*, 820366. https://doi.org/10.3389/fimmu.2022.820366.
146. Davis, N.M., Proctor, D.M., Holmes, S.P., Relman, D.A., and Callahan, B.J. (2018). Simple statistical identification and removal of contaminant sequences in marker-gene and metagenomics data. Microbiome *6*, 226. https://doi.org/10.1186/s40168-018-0605-2.
147. Segata, N., Izard, J., Waldron, L., Gevers, D., Miropolsky, L., Garrett, W.S., and Huttenhower, C. (2011). Metagenomic biomarker discovery and explanation. Genome Biol. *12*, R60. https://doi.org/10.1186/gb-2011-12-6-r60.
148. Inoue, Y., Izawa, K., Kiryu, S., Tojo, A., and Ohtomo, K. (2008). Diet and abdominal autofluorescence detected by in vivo fluorescence imaging of living mice. Mol. Imaging *7*, 21–27. https://doi.org/10.2310/7290.2008.0003.
149. Kwon, S., Davies-Venn, C., and Sevick-Muraca, E.M. (2012). In vivo dynamic imaging of intestinal motions using diet-related autofluorescence. Neuro Gastroenterol. Motil. *24*, 494–497. https://doi.org/10.1111/j.1365-2982.2012.01886.x.
150. Sun, Y., Zhong, X., and Dennis, A.M. (2023). Minimizing near-infrared autofluorescence in preclinical imaging with diet and wavelength selection. J. Biomed. Opt. *28*, 094805. https://doi.org/10.1117/1.jbo.28.9.094805.

STAR★METHODS

KEY RESOURCES TABLE

REAGENT or RESOURCE	SOURCE	IDENTIFIER
Antibodies		
Monoclonal rabbit anti-mouse CD45 antibody; clone D3F8Q	Cell Signaling Technology	Cat# 70257S, RRID:AB_2799780
Polyclonal rabbit anti-mouse NCR1 antibody	Abcam	Cat# Ab214468, RRID:AB_2814876
Monoclonal rabbit anti-mouse F4/80 antibody; clone D2S9R	Cell Signaling Technology	Cat# 70076S, RRID:AB_2799771
Monoclonal rabbit anti-mouse CD3ϵ antibody; clone E4T1B	Cell Signaling Technology	Cat# 78588S, RRID:AB_2889902
Monoclonal rabbit anti-mouse CD19 antibody; clone D4V4B	Cell Signaling Technology	Cat# 90176S, RRID:AB_2800152
Monoclonal rabbit anti-mouse Ly6G antibody; clone E6Z1T	Cell Signaling Technology	Cat# 87048S, RRID:AB_2909808
Bacterial and virus strains		
Escherichia coli GFP	American Type Culture Collection (ATCC)	ATCC #25922GFP
Chemicals, peptides, and recombinant proteins		
Lipopolysaccharide from *Escherichia coli* 0111:B4	Sigma Aldrich	Cat. L4391
Recombinant Human Interleukin 1-alpha	R&D Systems	Cat. 200-LA/CF
RU-486	Sigma Aldrich	Cat. M8046
Critical commercial assays		
ProcartaPlex Mouse Cytokine & Chemokine Panel 1A 36-plex	Invitrogen by Thermo Fisher Scientific	EPX360-26092-901
Deposited data		
16S rRNA gene sequencing files and metadata	NCBI Sequence Read Archive	PRJNA974164
Experimental models: Organisms/strains		
C57BL/6 mice	The Jackson Laboratory	Stock# 000664
Oligonucleotides		
TaqMan assays for RT-qPCR, see Table S4		
Software and algorithms		
GraphPad Prism v9.5.0	GraphPad	https://www.graphpad.com/features
ImageJ software	NIH	https://imagej.net/ij/
R Project	R Project	https://www.r-project.org/
Other		
QIAshredders	Qiagen	Cat# 79656
RNAlater stabilization solution	Invitrogen	Cat# AM7021
RNase-free DNase	Qiagen	Cat# 79254
RNeasy Mini Kit	Qiagen	Cat# 74104
SuperScript IV VILO master mix	Invitrogen	Cat# 11756050
DNeasy PowerLyzer Powersoil kit	Qiagen	Cat# 47014
MOVAT's Pentachrome Staining Kit	ScyTek Laboratories	Cat# MPS-1

RESOURCE AVAILABILITY

Lead contact

Further information and requests for resources and reagents should be directed to and will be fulfilled by the lead contact, Nardhy Gomez-Lopez (nardhy@wustl.edu).

Materials availability

This study did not generate new unique reagents.

Data and code availability

- 16S rRNA gene sequencing files and associated metadata have been uploaded to the National Center for Biotechnology Information's Sequence Read Archive (NCBI Sequence Read Archive: PRJNA974164).
- No unique code was generated during the study. Code supporting the study are available from the corresponding author.
- Any additional information required to reanalyze the data reported in this work is available from the lead contact upon request.

EXPERIMENTAL MODEL AND STUDY PARTICIPANT DETAILS

C57BL/6 mice were purchased from The Jackson Laboratory (Bar Harbor, ME, USA) and bred in the animal care facility at the C.S. Mott Center for Human Growth and Development at Wayne State University (Detroit, MI, USA). All mice were kept under a circadian cycle (light:dark = 12:12 h). Females, 8–12 weeks old, were bred with males and were checked daily between 8:00 a.m. and 9:00 a.m. for the appearance of a vaginal plug, which indicated 0.5 days *post coitum* (dpc). Females were then housed separately from the males and their weights were monitored daily. A weight gain of $\geq$2 g by 12.5 dpc confirmed pregnancy. All procedures were approved by the Institutional Animal Care and Use Committee (IACUC) at Wayne State University (Protocol No. 18-03-0584 and 21-04-3506). Different groups of mice were utilized in this study: 1) to establish the feasibility of evaluating the cervical length by ultrasound, 2) to evaluate the cervical shortening utilizing LPS-induced intra-amniotic inflammation, sterile intra-amniotic inflammation, or a progesterone blockade model of preterm birth, 3) to collect vaginal swab samples and harvest tissues for cytokine/chemokine evaluation, targeted gene expression, and histological analyses, and 4) to test whether preterm labor facilitates bacterial ascension from the cervico-vaginal space into the amniotic cavity.

METHOD DETAILS

Ultrasound evaluation of cervical length

Dams were anesthetized on 16.5 dpc by inhalation of 2% isoflurane [Fluriso™ (Isoflurane, USP) Vetone Boise, ID, USA] and 2 L/min of oxygen in an induction chamber, and a mixture of 1.5–2% isoflurane and 1.5–2 L/min of oxygen was used to maintain anesthesia. Mice were positioned on a heating pad, stabilized with adhesive tape, and fur was removed from the abdomen using Nair cream (Church & Dwight Co., Inc., Ewing, NJ, USA) as previously described.[13,15,16,18–22,101,136–139] Sterile forceps were utilized to expose the vulva, and 150 μL of Sterile Aquasonic® 100 ultrasound transmission gel (Parker laboratories, Fairfield, NJ, USA), was administered into the vagina, creating contrast to clearly detect the external limit of the uterine cervix (i.e., external os). First, a 3D reconstruction of the cervix was performed utilizing the 3D motor stage of the Vevo® 2100 Imaging System (VisualSonics Inc., Toronto, Ontario, Canada). For cervical length measurement, the ultrasound probe was positioned sagittal in relation to the long axis of the abdomen and mobilized with a mechanical holder. The cervix was positioned in a longitudinal view. Cervical length was measured from the internal to the external limit of the cervix, at least three times per mouse, and its average was utilized as the final value for cervical length. Cervical shortening was calculated as the percentage of reduction of the cervical length between an initial evaluation before the intra-amniotic or subcutaneous injection and 6 h [signs of early labor (SEL), corresponding to the earliest timepoint when cervical shortening can be accurately determined] or 12 h [signs of active labor (SAL), corresponding to the timepoint closest to the earliest preterm delivery] later.

Ex vivo measurement of cervical length

Mice were euthanized on 16.5 dpc immediately after the ultrasound measurement of the cervical length and placed in a dissection pad. The midline of the abdomen and peritoneum were opened, the bladder was pulled down, and the adipose tissue surrounding the cervix and vagina, as well as the rectum were removed. The pubic symphysis was cut and the anterior wall of the vagina was opened longitudinally until the visualization of the external os of the cervix. The vaginal tissue surrounding the cervix was carefully dissected, and the internal os was identified and sectioned. The extracted cervix was photographed next to a ruler that was utilized as a reference to calculate the cervical length using ImageJ (NIH, Bethesda, MD, USA). The calculation of the cervical length in the tissues was done by two independent investigators, and their average was utilized for the comparison with the cervical length obtained by the ultrasonographic approach.

Ultrasound-guided intra-amniotic injections

On 16.5 dpc, mice were anesthetized as described above. The ultrasound-guided intra-amniotic injection of lipopolysaccharide of *Escherichia coli* O111: B4 (LPS, Sigma-Aldrich, St. Louis, MO, USA) at a concentration of 100 ng dissolved in 25 μL of sterile 1X phosphate-buffered saline (PBS; Life Technologies, Grand Island, NY, USA), IL-1α (Cat. 200-LA/CF, R&D Systems, Inc., Minneapolis, MN, USA) 100 ng per 25 μL of sterile PBS was performed in each amniotic sac using a 30-G needle (BD PrecisionGlide Needle; Becton Dickinson, Franklin Lakes, NJ, USA). Control dams were injected with 25 μL of sterile PBS. Successful intra-amniotic injection was verified by using color Doppler ultrasound to identify the "injection jet sign".[21,24,102] After ultrasound completion, mice were placed under a heating lamp for recovery, which was defined as when the mouse resumed normal activities, such as walking and responding, and typically occurred within 5 min after removal from anesthesia. A first group of mice was utilized to evaluate the time from injection to delivery to establish the timepoints for SEL and SAL. To reduce the number of

mice, observational data from dams injected with PBS or IL-1α was taken from a separate study that was conducted from our group at the same time and in the same institution as the observational experiments included herein.[20]

Subcutaneous injections of RU-486

Dams were injected subcutaneously (s.c.) on 16.5 dpc with 150 mg/100 μL of RU-486 (Sigma Aldrich) dissolved in DMSO (Sigma-Aldrich) and diluted 1:13 in PBS, or 100 μL of DMSO diluted 1:13 in PBS as a control.

Video monitoring

Pregnancy outcomes were recorded *via* video camera (Sony Corporation, Tokyo, Japan) to determine gestational length and rate of preterm birth. Preterm birth was defined as delivery occurring before 18.5 dpc and its rate was represented by the percentage of females delivering preterm among the total number of mice injected.

Sampling of maternal-fetal tissues for molecular and histologic experiments

Pregnant mice received an intra-amniotic injection of LPS, IL-1α, or PBS or subcutaneous injection of RU-486 or DMSO on 16.5 dpc. Mice were euthanized with SEL (6 h after administration of stimuli) or SAL (12 h after administration of the stimuli) for tissue collection. The amniotic fluid was collected from each amniotic sac and centrifuged at 1,300 × g for 5 min at 4°C. The resulting supernatants were stored at −20°C until analysis. After dissection of the uterine horns, the vaginal tissue was carefully removed, and the upper limit of the cervix was incised to isolate the cervical tissue. The cervix and vagina were preserved in RNA*later* Stabilization Solution (Cat# AM7021; Invitrogen by Thermo Fisher Scientific, Carlsbad, CA, USA), according to the manufacturer's instructions, and stored at −80°C until RNA extractions for reverse transcription-quantitative polymerase chain reaction (RT-qPCR). Tissues for histological analyses were fixed in 10% Neutral Buffered Formalin (Surgipath, Leica Biosystems, Wetzlar, Germany) and embedded in paraffin. Five-μm-thick sections were cut and mounted on Superfrost® Plus microscope slides (Cat. No. 48311-703, VWR International, LLC. Radnor, PA, USA).

Determination of cytokine concentrations in amniotic fluid

The concentrations of cytokines/chemokines in the murine amniotic fluid were determined using the ProcartaPlex Mouse Cytokine & Chemokine Panel 1A 36-plex (Invitrogen by Thermo Fisher Scientific), according to the manufacturer's instruction, to determine: IFN-α, IFN-γ, IL-12p70, IL-1β, IL-2, TNF, GM-CSF, IL-18, IL-17A, IL-22, IL-23, IL-27, IL-9, IL-15/IL-15R, IL-13, IL-4, IL-5, IL-6, IL-10, Eotaxin (CCL11), IL-28, IL-3, LIF, IL-1α, IL-31, GRO-α (CXCL1), MIP-1α (CCL3), IP-10 (CXCL10), MCP-1 (CCL2), MCP-3 (CCL7), MIP- 1β (CCL4), MIP-2 (CXCL2), RANTES (CCL5), G-CSF, M-CSF, and ENA-78 (CXCL5). An FLEXMAP 3D (Luminex Corporation, Austin, TX, USA) was used to read the plates and the concentrations of analytes were calculated using the Xponent version 4.2 (Luminex). The sensitivities of the assays were 3.03 pg/mL (IFN-α), 0.09 pg/mL (IFN-γ), 0.21 pg/mL (IL-12p70), 0.14 pg/mL (IL-1β), 0.10 pg/mL (IL-2), 0.39 pg/mL (TNF), 0.19 pg/mL (GM-CSF), 9.95 pg/mL (IL-18), 0.08 pg/mL (IL-17A), 0.24 pg/mL (IL-22), 2.21 pg/mL (IL-23), 0.34 pg/mL (IL-27), 0.28 pg/mL (IL-9), 0.42 pg/mL (IL-15/IL-15R), 0.16 pg/mL (IL-13), 0.03 pg/mL (IL-4), 0.32 pg/mL (IL-5), 0.21 pg/mL (IL-6), 0.69 pg/mL (IL-10), 0.01 pg/mL (Eotaxin/CCL11), 20.31 pg/mL (IL-28), 0.11 pg/mL (IL-3), 0.28 pg/mL (LIF), 0.32 pg/mL (IL-1α), 0.45 pg/mL (IL-31), 0.05 pg/mL (GRO-α/CXCL1), 0.13 pg/mL (MIP-1α/CCL3), 0.26 pg/mL (IP-10/CXCL10), 3.43 pg/mL (MCP-1/CCL2), 0.15 pg/mL (MCP-3/CCL7), 1.16 pg/mL (MIP-1β/CCL4), 0.37 pg/mL (MIP-2/CXCL2), 0.35 pg/mL (RANTES/CCL5), 0.19 pg/mL (G-CSF), 0.02 pg/mL (M-CSF), and 5.67 pg/mL (ENA-78/CXCL5).

DNA extraction from vaginal swab samples

Vaginal samples were taken utilizing FLOQSwabs® (COPAN diagnostics, Murrieta, CA, USA). An initial vaginal swab was collected in the absence of labor, prior to the administration of the stimulus to induce preterm labor (T0). Dams were then intra-amniotically injected with PBS, LPS, or IL-1α, or subcutaneously with DMSO or RU-486, and a second vaginal swab was collected with signs of early premature labor (SEL; 6 h). The same procedure was performed in a second group of mice, except that the second vaginal swab was taken with signs of active labor (SAL; 12 h). Therefore, both the SEL and SAL groups of mice were only sampled twice. All swab samples collected for 16S rRNA gene sequencing were stored at −80°C until DNA extractions were performed. All extractions were performed within a biological safety cabinet with personnel donning a sterile gown, sterile sleeves, sterile gloves, and a facial mask.

Genomic DNA was extracted from vaginal swab samples (and blank extraction kit controls) using the DNeasy PowerLyzer Powersoil kit (Qiagen, Germantown, MD, USA), with minor modifications to the manufacturer's protocols as previously described.[140–142] Specifically, 400 μL of Powerbead solution, 200 μL of phenol:chloroform:isoamyl alcohol (pH 7–8), and 60 μL of preheated solution C1 were added to the provided bead tubes following UV treatment. Next, vaginal swabs were added to the tubes. Tubes were briefly vortexed, and cells mechanically lysed in a bead beater for two rounds of 30 sec each. Supernatants were transferred to new tubes, following 1 minute of centrifugation, and 1 μL of PureLinkTM Rnase A (Invitrogen), 100 μL of solution C2, and 100 μL of solution C3 were added. Tubes were then incubated at 4°C for 5 min. Lysates were transferred to new tubes containing 650 μL of C4 solution and 650 μL of 100% ethanol after a 1 min centrifugation. Lysates were then loaded onto filter columns 635 μL at a time, centrifuged for 1 min, and the flowthrough discarded. To ensure all lysate passed through the filter columns, this wash process was repeated three times. After the wash steps, 500 μL of solution C5 were loaded into the filter columns and centrifuged for 1 min. The flowthrough was discarded, and then to dry the filter columns, the tubes were centrifuged for 2 min. After transferring the spin columns to clean 2.0 mL collection tubes, 60 μL of pre-heated solution C6 were added directly to

the center of the columns. Following a 5 min room temperature incubation, the tubes were centrifuged for 1 min to elute the purified DNA. Purified DNA was then transferred to new 2.0 mL collection tubes and stored at −20°C.

16S rRNA gene sequencing of swab samples

The V4 region of the 16S rRNA gene was amplified and sequenced via the dual indexing barcode method conceived by Kozich et al.[143] Forward and reverse primers were 515F: 5′-GTGCCAGCMGCCGCGGTAA-3′ and 806R: 5′-GGACTACHVGGGTWTCTAAT-3′, respectively. Twenty microliter PCR reactions were performed containing 0.75 μM of each primer, 3.0 μL DNA template, 10.0 μL of DreamTaq High Sensitivity Master Mix (Thermo Scientific, Waltham, MA, USA), and 5 μL of DNase-free water. Reaction conditions were as follows: 95° for 3 min, followed by 30 cycles of 95°C for 45 sec for vaginal swabs, 50°C for 60 sec, and 72°C for 90 sec, with an additional elongation at 72°C for 10 min. A Qubit 3.0 fluorometer and Qubit dsDNA assay kit (Life Technologies, Carlsbad, CA, USA) were then used to quantify the DNA, following the manufacturer's protocol. Samples were pooled in equimolar concentrations and purified using the Cytiva Sera-Mag Select DNA Size Selection and PCR Clean-Up Kit (Global Life Sciences, Little Chalfont, Buckinghamshire, UK), according to the manufacturer's instructions. Illumina MiSeq sequencing was performed at the Michigan State University Research Technology Support Facility Genomics Core. Specifically, sequencing was achieved in a 2 × 250bp paired end format using a 500 cycle v2 reagent cartridge. Due to sample sizes, samples from SEL mice and SAL mice, and their respective controls, were sequenced on separate runs, and therefore all downstream processing was performed with sequence data grouped by SEL or SAL. Raw sequence reads were processed, classified, and converted to amplicon sequence variants (ASV), defined by 100% sequence similarity using DADA2 (v 1.12)[144] and the online MiSeq protocol with minor modifications, as previously described.[145] The R package decontam[146] was used to identify ASVs as background DNA contaminants by comparing biological samples to technical controls with the *isContaminant* function. After assessing the distribution of decontam scores, a threshold cutoff of 0.75 was used for the SEL dataset and 0.70 for the SAL dataset, which resulted in the classification of 296/1004 and 210/1184 ASVs as background DNA contaminants, respectively.

Samples were only included in microbiome analyses if their profiles had at least 826 or 915 quality-filtered 16S rRNA gene sequences for the SEL and SAL datasets, respectively. For alpha diversity analyses, samples were randomly subsampled to the minimum read depth for each respective dataset and alpha diversity indices (Chao1, Shannon, Inverse Simpson) were calculated with the phyloseq package (v 1.34.0) in R. Alpha diversity comparisons were made using t-tests, Mann-Whitney tests, or their paired equivalents, as was appropriate, with the rstatix package (v 0.7.0) in R. Beta diversity comparisons were made using Jaccard (i.e., composition) or Bray-Curtis (i.e., structure) similarity indices and the adonis function in the vegan package (v. 2.5.7) in R. Linear Discriminant Analysis Effect Size (LefSe)[147] analyses were used to identify differentially abundant bacterial taxa between sampled timepoints for treatment and control groups. For LefSe, default settings were used and analyses were performed through the Huttenhower lab Galaxy server (https://huttenhower.sph.harvard.edu/galaxy/) after removing singletons. Alpha diversity plots were generated with the ggplot2 package (v 3.3.5) in R. Beta diversity plots were generated using base R (v 4.0.3) and additional ordination was added using vegan. Heatmaps were generated using the gplots package (v 3.1.1) in R.

Characterization of cervical tissue using movat pentachrome staining

The Movat Pentachrome Staining Kit (ScyTek Laboratories, Inc., Logan, UT, USA) was used to characterize the presence of elastin, collagen, muscle, and mucin on cervical tissue collected from mice injected with either PBS, LPS, IL-1α, DMSO, or RU-486. The tissue slides were deparaffinized and rinsed in tap and distilled water. Then, the slides were incubated in Elastin Stain Solution for 20 min, 2% ferric chloride for 10 sec, 5% sodium thiosulfate solution for 1 min, Alcian Blue Solution for 25 min, Biebrich Scarlet-Acid Fuchsin Solution for 2 min, phosphotungstic acid solution 7 min (twice), and 1% acetic acid solution for 3 min. Slides were rinsed in distilled water between each incubation listed above. Next, excess acetic acid solution was removed, and the slides were stained with Yellow Stain Solution for 15 min. Images were taken with the Vectra Polaris Multi Spectral Imaging (MSI) System (PerkinElmer, Hopkinton, MA, USA) using brightfield setting.

Leukocyte detection using DAB immunohistochemistry

Tissue slides were deparaffinized by xylene, which was removed by 100% alcohol, rehydrated through a series of alcohol dilutions. CD45 (monoclonal rabbit anti-mouse CD45 antibody; clone D3F8Q; Cat. 70257S, Cell Signaling Technology, Danvers, MA, USA) immunohistochemistry staining was performed using a Leica Bond Max Automatic Staining System and leukocytes were detected through the oxidation of 3,3′-diaminobenzidine (DAB) from the Bond Polymer Refine Detection Kit (both from Leica Microsystems, Wetlzar, Germany). Images were scanned using the Vectra Polaris MSI System with brightfield setting.

OPAL multiplex immunofluorescence

OPAL multiplex immunofluorescence staining of cervical tissue was performed using the OPAL multiplex 7-color IHC kit (Cat. NEL811001KT; Akoya Biosciences, Marlborough, MA, USA). Tissue slides were deparaffinized by xylene, which was removed by 100% alcohol and rehydrated with a series of alcohol dilutions. After deparaffinization, the slides were briefly rinsed in deionized water, submerged in an appropriate antigen retrieval (AR) buffer, and boiled in a microwave oven. Non-specific Ab binding was blocked by incubating the tissue in OPAL antibody diluent/blocking (Cat. ARD1001EA, Akoya Biosciences) solution for 10 min prior to the addition of the antibody. Following optimization, the detection panel was generated in the following order (antibody followed by OPAL fluorophore): NCR1 (polyclonal rabbit anti-mouse antibody; cat. Ab214468, Abcam, Cambridge, England) with OPAL 520, F4/80 (monoclonal rabbit anti-mouse antibody; clone D2S9R; cat.

70076S, Cell Signaling Technology, MA, USA) with OPAL 540, CD3ϵ (monoclonal rabbit anti-mouse antibody; clone E4T1B; cat. 78588S, Cell Signaling Technology) with OPAL 570, CD19 (monoclonal rabbit anti-mouse antibody; clone: D4V4B; cat. 90176S, Cell Signaling Technology) with OPAL 620, and Ly6G (monoclonal rabbit anti-mouse antibody; clone E6Z1T; cat. 87048S, Cell Signaling Technology) with OPAL 690. After incubation with Ab for 1 h in room temperature, the slides were rinsed in tris-buffered saline and Tween 20 (TBST) and incubated with horseradish peroxidase conjugated secondary antibody (Cat. ARR1001HT; Akoya Biosciences) for signal amplification. The slides were rinsed in TBST again and incubated with OPAL fluorophore. Cycles of antigen retrieval, antibody incubation, and signal amplification were repeated in the order described above. After Ly6G and OPAL 690 staining, the slides were boiled before incubation with DAPI for nuclear staining and mounted with AquaSlip Aqueous Mounting Medium (Cat. MMC0619, American MasterTech). Images were acquired using the Vectra Polaris MSI System at 20× magnification and analyzed using Inform software version 2.6.0 (PerkinElmer).

RNA isolation, cDNA synthesis, and reverse transcription-quantitative PCR analysis

Total RNA was isolated from the cervical and vaginal tissues using QIAshredders (Qiagen, Hilden, Germany), RNase-free DNase (Qiagen), and RNeasy Mini kits (Qiagen) according to the manufacturer's instructions. The concentration of the RNA was measured with a NanoDrop 8000 spectrophotometer (Thermo Scientific, Wilmington, DE, USA), and the RNA integrity was assessed using a Bioanalyzer 2100 (Agilent Technologies, Wilmington, DE, USA) for each sample. Complementary (c)DNA was synthesized by using SuperScript™ IV VILO™ Master Mix (Invitrogen by Thermo Fisher Scientific Baltics UAB, Vilnius, Lithuania) following to the manufacturer's instructions. Gene expression was determined on the BioMark System for high-throughput RT-qPCR (Fluidigm, San Francisco, CA, USA) using the TaqMan gene expression assays listed in Table S4.

Escherichia coli GFP growth

Escherichia coli GFP (ATCC #25922GFP; American Type Culture Collection (ATCC), Manassas, VA, USA) was cultivated in Luria-Bertani (LB) broth (Teknova Inc., Hollister, CA, USA) at 37°C in rotatory motion. An overnight culture was diluted into fresh medium and grown to the mid-logarithmic phase (OD_{600} was between 0.9 and 1.0). Next, bacteria were adjusted to 1×10^8 cells/40 μL and harvested by centrifugation at 3,700 × g for 10 minutes and re-suspended in PBS (Life Technologies, Paisley, UK) to be administered intra-vaginally.

Ultrasound-guided intra-vaginal administration of *Escherichia coli* GFP

A new group of mice was randomized to receive ultrasound-guided intra-amniotic injection of LPS, IL-1α, or PBS, or subcutaneous injections of RU-486 or DMSO, as described above. Immediately after the intra-amniotic or subcutaneous injection of the stimuli, with the dams still under anesthesia, 1×10^8 cells/40 μL of *E. coli* GFP or 40 μL of PBS as a negative control were administered next to the external os of the cervix under ultrasound visualization using a 18G blunt needle (BD Blunt Fill needle, Becton Dickinson). This strategy was utilized to assure that the *E. coli* GFP was present in the vagina in the absence of cervical shortening. Thus, when the process of preterm labor began, the bacteria would already be in the vagina.

IVIS imaging

Anesthetized dams were imaged using the IVIS Spectrum *in vivo* imaging system (Perkin Elmer, Waltham, MA, USA). An excitation filter of 491 nm and an emission filter of 509 nm were used to determine GFP expression. It is well documented that mouse chow can interfere with fluorescence imaging, given that the alfalfa component contains chlorophyll and thus the gastrointestinal tract could emit autofluorescence.[148–150] To reduce the autofluorescence background, a group of mice was injected with either PBS, LPS, IL-1α, DMSO, or RU-486, followed immediately by intra-vaginal administration of PBS. This group was utilized as a negative control to set the color scale for fluorescence imaging experiments. After abdominal imaging, dams were euthanized and a second set of images of the intra-peritoneal cavity was taken after removing the skin and peritoneum. Next, the amniotic fluid was collected into sterile tubes, which were also imaged together with a tube containing only PBS as control.

QUANTIFICATION AND STATISTICAL ANALYSIS

Cervical shortening, cytokine concentrations, gene expression, and histology data were analyzed with GraphPad Prism version 9.5.0 for Windows (GraphPad Software, San Diego, California, USA, www.graphpad.com). The Mann-Whitney *U*-test was used for comparing cervical shortening and amniotic fluid cytokine/chemokine concentration. Mann-Whitney *U*-tests or unpaired *t*-tests were used for comparing gene expression between study groups. Unpaired *t*-tests were utilized for comparing the infiltration of leukocyte in the cervix. For qPCR analysis, negative delta threshold cycle ($-\Delta C_T$) values were determined using multiple reference genes (*Gusb*, *Hsp90ab1*, *Gapdh*, and *Actb*) averaged within each sample to determine gene expression levels. The $-\Delta C_T$ values were normalized by calculating the *Z* score of each gene, and then heatmaps were created in GraphPad Prism, which represent the mean of the *Z* score of $-\Delta C_T$. A p value ≤ 0.05 was considered statistically significant. General microbiome data analysis was performed using R (v.4.2.2; https://www.r-project.org/), as described above. The statistical details for each experiment are described in the corresponding figure legends, including statistical tests used, definitions of n values, definition of center, and dispersion/precision measures.